



ELSEVIER

Precambrian Research 112 (2001) 303–329

**Precambrian  
Research**

www.elsevier.com/locate/precamres

# Dolomitization and isotope stratigraphy of the Vazante Formation, São Francisco Basin, Brazil

Karem Azmy<sup>a</sup>, Jan Veizer<sup>a,b</sup>, Aroldo Misi<sup>c</sup>, Tolentino Flávio de Oliveira<sup>d</sup>,  
Andreia Lima Sanches<sup>c</sup>, Marcel Auguste Dardenne<sup>e</sup>

<sup>a</sup> Ottawa-Carleton Geoscience Center, University of Ottawa, Ottawa, Ont., Canada K1N 6N5

<sup>b</sup> Institut für Geologie, Mineralogie und Geophysik, Ruhr Universität, 44780 Bochum, Germany

<sup>c</sup> Centro de Pesquisa em Geofísica e Geologia e Curso de Pós-Graduação em Geologia, Instituto de Geociências/CPGG,  
Universidade Federal da Bahia, Salvador, Bahia 40210-340, Brazil

<sup>d</sup> Cia Mineira de Metais, P.O. Box # 1, 38780 Vazante MG, Brazil

<sup>e</sup> Instituto de Geociências, Universidade de Brasília, DF 70910-900, Brazil

Received 9 September 1999; accepted 26 April 2001

## Abstract

The Vazante Formation consists of approximately 1700 m of mainly microbial mats and stromatolitic reefal lenses that were deposited on shallow marine platform and have been entirely dolomitized. Samples representing different dolomite generations were taken from three boreholes covering the entire spectrum of the Vazante carbonates. Dolomites can be classified, based on petrography and geochemistry, into four generations ranging in crystal size between  $\sim 4 \mu\text{m}$  (almost micritic) and 3 mm and occurring as both replacements and cements. The Sr/Ca molar ratios, calculated for the dolomitizing fluid (0.0006–0.0138), suggest a contribution from a non-marine, possibly meteoric, water component. The  $\delta^{18}\text{O}$  and  $\delta^{13}\text{C}$  values vary from  $-0.1$  to  $-14.3\text{‰}$  (PDB) and  $0.2$  to  $-2.3\text{‰}$  (PDB), respectively. Fluid-inclusion study suggests that dolomitization must have commenced at a temperature lower than about  $50 \text{ }^\circ\text{C}$ . A mixing-zone model of dolomitization for Dolomites I–III satisfies the constraints from elemental chemistry,  $\delta^{18}\text{O}$ ,  $^{87}\text{Sr}/^{86}\text{Sr}$  and fluid inclusions. The petrographic and chemical criteria of the latest generation, Dolomite IV, reflect conditions of deep burial environment at temperatures above  $120\text{--}130 \text{ }^\circ\text{C}$ . The  $\delta^{13}\text{C}$  values show only small variations at the base of the formation, followed by a major negative plunge ( $\sim 4\text{‰}$ ) at the top, this plunge correlated with the Sturtian glacial phase. In contrast to C-isotopes, only few samples may have retained their near-primary  $^{87}\text{Sr}/^{86}\text{Sr}$  values of  $0.70614\text{--}0.70734$ . The lowest  $^{87}\text{Sr}/^{86}\text{Sr}$  value ( $0.70614$ ), from fibrous cement in the upper part of the formation, correlates with the negative  $\delta^{13}\text{C}$  shift and is also consistent with the Sr-isotope signature proposed for the glacial Sturtian seawater. The  $\delta^{34}\text{S}$  values, obtained from sulfates trapped in carbonates, range between  $10.8$  and  $16.9\text{‰}$  with a jump to  $21.3\text{‰}$  in the overlying formation. All isotope signals are within the range suggested for the early Neoproterozoic seawater, but the Precambrian baseline is poorly known and additional work is required to confirm this tentative assignment. © 2001 Elsevier Science B.V. All rights reserved.

**Keywords:** Proterozoic carbonates; Dolomites; Geochemistry; Isotope stratigraphy; Vazante Formation; Brazil

\* Corresponding author. Present address: Department of Geoscience, University of Nevada, 4505 Maryland Parkway, Las Vegas, NV 89154-4010, USA. Tel.: +1-702-8951239; fax: +1-702-8954064.

E-mail address: azmyk@hotmail.com (K. Azmy).

## 1. Introduction

The Vazante Formation of São Francisco Basin, east-central Brazil (Fig. 1) is composed of shallow shelf deposits, with dolostones predominant. Despite the fact that dolomitic sequences are ubiquitous in the Precambrian of South America, and elsewhere, they have been, in contrast to their Phanerozoic counterparts (cf. Machel and Mountjoy, 1986; Tucker and Wright 1990; Budd, 1997), rarely subjected to detail geochemical studies. This is also the case for the Vazante Formation where previous studies dealt mainly with the stratigraphy, lithofacies and sedimentary environments (e.g. Madalosso, 1979; Rigobello et al., 1988; Freitas-Silva and Dardenne, 1992), but not with the geochemistry of dolostones.

The main objectives of this paper are: (1) to define and characterize the different generations of Vazante dolomites; (2) to study their paragenetic sequence and geochemical attributes in relation to burial history; (3) to constrain the sources and chemistry of dolomitizing solutions; and (4) to establish a reliable isotope stratigraphic profile for the Vazante Formation that may provide a refined age estimate and advance the issue of its correlation with other Neoproterozoic sequences in the area and beyond.

## 2. Geological setting

The São Francisco Craton (SFC) in east-central Brazil (Fig. 1) is an important geotectonic unit of South American continent because of its geological diversity and mineral resources. With 32% of the proven reserves of metallic ores and 24% of the total mineral production of Brazil, it hosts giant deposits of iron, manganese, niobium, magnetite, gold and zinc, among others.

The SFC is formed by an Archean-Paleoproterozoic basement, with high grade metamorphic rocks intruded by granites, and by low to medium grade volcanosedimentary and greenstone belts sequences (Almeida et al., 1976). These units are covered by well preserved Meso- and Neoproterozoic sedimentary strata represented

by: (a) The Mesoproterozoic Espinhaço and Chapada Diamantina Groups, with continental acidic volcanics at the base and sandstones, siltstones, shales and subordinate dolostones in the middle and upper sections; and (2) The presumably Neoproterozoic, mostly carbonate, sequences. The present configuration of the SFC is believed to have been shaped by the Brazilian–Pan African Orogeny (Almeida and Hasui, 1984) that climaxed ~ 600–550 Ma ago.

The ‘Neoproterozoic’ assemblages consist mostly of carbonate platform sediments within the São Francisco, Irecê and Una-Utinga basins (Fig. 1) and of metasediments in the fold belts around the cratonic area. Overall, they cover more than 300 000 km<sup>3</sup> of the SFC. From base to top, they usually consist of the following lithostratigraphic assemblages:

1. Glacigenic units: Diamictites, conglomerates, pelites and quartzitic (arkosic) lenses of the Jequitáí, Macaúbas and Bebedouro Formations. Although predominantly glacigenic, the units also contain glacio-marine and fluvial sediments.
2. Carbonate platform sediments: Limestones, dolostones, marls, shales and siltstones. In the São Francisco Basin, the sequence is known as the Bambuí Group and contains carbonate sediments of the Sete Lagoas and Lagoa do Jacaré Formations deposited in a warm shallow shelf environment. The correlative unit in the Irecê and Una-Utinga Basins is the Salitre Formation of the Una Group. In the western part of the SFB, separated from the Bambuí Group by the Paranoá Basin, crops out the Vazante Formation. In the marginal fold belts, particularly in the Brasília Fold Belt, the latter reaches up to ~ 2000 m thickness. The formation consists entirely of dolostones with abundant stromatolites (Dardenne, 1978; Madalosso, 1979; Rigobello et al., 1988), including *Conophyton metulum* and *C. cf. cylindricum*, that were described also from sediments that are stratigraphically below the Bambuí Group (Dardenne and Walde, 1979; Karfunkel and Hoppe, 1988; Fairchild et al., 1996).

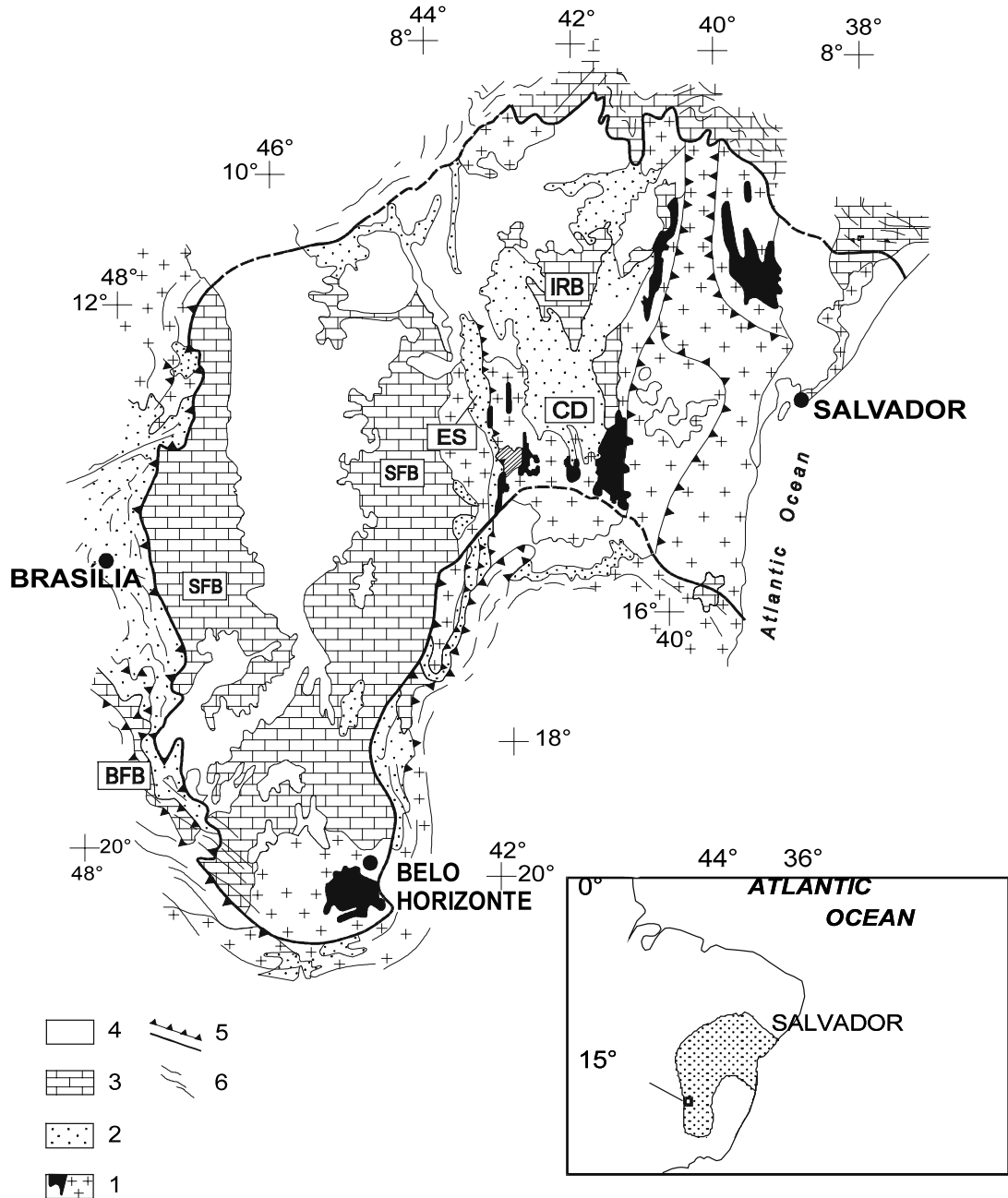


Fig. 1. Location map of the Vazante area in São Francisco Basin, Brazil (modified after Alkmim et al., 1993). Explanations: BFB, Brasília Fold Belt; CD, Chapada Diamantina; ES, Espinhaço; IRB, Irecê Basin; SFB, São Francisco Basin; UVB, Una-Utinga Basin; (1) Archean-Paleoproterozoic basement and in black, greenstone belts and volcano-sedimentary sequences; (2) Mesoproterozoic sedimentary cover (Espinhaço Supergroup); (3) Neoproterozoic sedimentary cover (Bambui Group and correlative sequences); (4) Phanerozoic cover; (5) Craton limits; and (6) Folded belts.

3. Molasse-type strata: Arkosic sandstones, siltstones, phyllites and conglomerates, probably related to the evolution of a post-tectonic 'molasse-type' basin (Thomaz Filho et al., 1998). In the Minas Gerais state they are represented by the Três Marias Formation.

### 3. Age assignment and correlation problems

Based on the occurrence of *C. metulum* stromatolites, Cloud and Dardenne (1973) suggested that the sedimentation of the Vazante Formation could have occurred 1350–900 Ma ago, predating the sedimentation of the Bambuí Group. The latest published geological map of the Minas Gerais state (Pedrosa Soares et al., 1994) still assigns the Vazante Formation to the Mesoproterozoic.

Karfunkel and Hoppe (1988) proposed a scenario for the evolution of the SFC, where all glacial units in central-eastern Brazil are believed to be younger than the Archean basement and the Early to Middle Proterozoic rocks, and older than the carbonates of the Bambuí Group and its correlatives. In this scenario, the craton with its preglacial deposits was uplifted, depositing diamictites during continental glaciation. Subsequent subsidence, associated with global warming and transgression, led to deposition of the younger shallow water sediments of the Bambuí Group and its correlatives. The glacial deposits are therefore believed to correlate with the Neoproterozoic Sturtian glaciation event (Dardenne, 1979; Karfunkel and Hoppe, 1988), with carbonates (including the Vazante Formation) somewhat younger than the glacial deposits.

Radiometric dating, unfortunately, did not as yet provide clear resolution to this dilemma. The early Rb/Sr dating of argillaceous sediments of the Vazante Formation (Amaral and Kawashita, 1967) yielded  $600 \pm 50$  Ma estimate, but this age was attributed to the Brazilian orogeny. Subsequently, Macedo and Bonhomme (1984) published an apparent Rb/Sr age of 800 Ma for argillaceous sediments of the Salitre Formation (Una Group). In contrast, Rb/Sr 'ages' for the Bambuí fine-grained siliciclastic sediments from

the SFB in the Minas Gerais state ranged from 590 to 640 Ma (Parenti Couto et al., 1981; Thomaz Filho and Lima, 1981), in accord with the  $< 680$  Ma Pb/Pb estimates based on galena from Vazante-Paracatu area and from carbonates of the Bambuí Group in the southern part of the SFB (Iyer et al., 1992, 1995). Other Pb/Pb estimates from the latter area (Babinski et al., 1999; D'Agrella-Fihlo et al., 2000), on the other hand, claim that the carbonate sequence has a minimum depositional age of  $686 \pm 69$  Ma. The subsequent overprinting by the late Proterozoic Brazilian Orogeny that deformed and metamorphosed sediments in many parts of the SFB (Lagoeiro, 1990; Alkmim et al., 1993; Chemale et al., 1993) does not make the issue of age and stratigraphic correlations anymore tractable.

Chemostratigraphy is becoming an alternate correlation tool, and its utility has been documented for the Phanerozoic (e.g. McArthur, 1994; Veizer et al., 1997, 1999; Azmy et al., 1999) as well as the Precambrian (e.g. Derry et al., 1989; Fairchild et al., 1990; Kaufman et al., 1991; Knoll and Walter, 1992; Kaufman and Knoll, 1995). In addition, such isotope proxy signals can be utilized also for alternate purposes, such as paleoclimatic modelling (e.g. Kaufman et al., 1993; Hoffman et al., 1998). Reconnaissance chemostratigraphic studies ( $\delta^{13}\text{C}$ ,  $\delta^{18}\text{O}$ ,  $^{87}\text{Sr}/^{86}\text{Sr}$ ,  $\delta^{34}\text{S}$ ) of carbonates from the Bambuí group and its correlative Una Group in the Irecê basin suggested an age of  $\sim 600$ – $670$  Ma (Misi et al., 1997; Kawashita, 1998; Misi and Veizer, 1998) for the carbonates above the glacial units.

As a tentative conclusion, the radiometric and chemostratigraphic considerations appear to favour a Neoproterozoic age for carbonate sequences above glacial sediments, although more precise assignment is clearly an open question. The reported existence of diamictites in the Coromandel unit (Dardenne et al., 1998), stratigraphically directly below the Serra de Garotte Formation (Fig. 2), supports such an assignment also for the Vazante Formation. For the latter, this would contradict the evidence for Mesoproterozoic age based on the presence of *C. metulum*. Alternatively, the Vazante Formation is Mesoproterozoic and thus not a correlative unit

of the Bambuí Group. An attempt to resolve this conundrum by isotope stratigraphy is one of the hoped for goals of this contribution.

#### 4. Methodology

Four cores, provided by the Brazilian mining company Cia Mineira de Metais (detailed description available from De Oliveira), covering a total of 2330 m and encompassing all carbonate units of the Vazante Formation as well as the lowermost part of the overlying Lapa Formation (Fig. 2) were studied. These cores are CMM-244 (N = 8013184,18; E = 303422,62; COTA = 722,00), CMM-279 (N = 8016754,20; E = 303945,14; COTA = 693,99), CMM-500 (N = 8014221,29; E = 302323,90; COTA = 719,94) and KVD-F60 (N = 8033644,60; E = 310885,37; COTA = 671,53). They were selected with an intention to avoid, as much as possible, tectonic complications in the area. In addition, two samples from limestone interbeds in the underlying Serra do Garrote Formation were also collected from outcrops in the field. Thin sections of the samples were examined petrographically under standard polarizing microscope and lumnoscope and stained with Alizarin Red-S and potassium ferricyanide solutions (Dickson, 1966). A mirror-image slab of each thin section was also prepared and polished to be used for microsampling. Cathodoluminescence (CL) was performed using a Technosyn 8200 MKII cold cathode instrument operated at ~11 kV accelerating voltage and ~450 mA gun current intensity. Randomly selected samples were analyzed by XRD to ensure that dolomites did not contain vestiges of a CaCO<sub>3</sub> precursor.

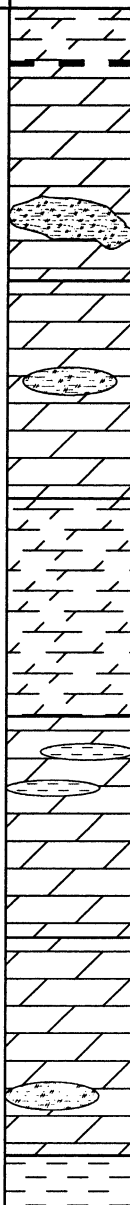
Samples representing successive dolomite generations were selected for geochemical analysis. Powder samples, each ~10 mg, microsampled from clean slabs that were washed with deionized water and dried overnight at 50 °C, were drilled by a low-speed microdrill. For oxygen and carbon isotope analysis, about 4 mg samples were reacted under vacuum overnight with ~1 ml of ultrapure orthophosphoric acid at 50 °C in a water bath (cf. Azmy et al., 1998). The produced CO<sub>2</sub> was analysed using the VG Isogas SIRA-12 triple

collecting mass spectrometer at the G. G. Hatch Isotope Laboratory, University of Ottawa. The laboratory standards were NBS-18 ( $\delta^{18}\text{O} = -23.00\text{‰}$  and  $\delta^{13}\text{C} = -5.00\text{‰}$  PDB) and NBS-19 ( $\delta^{18}\text{O} = -2.20\text{‰}$  and  $\delta^{13}\text{C} = +1.95\text{‰}$  PDB) with a routine precision ( $2\sigma$ ) for a pure carbonate samples of 0.1‰.

The residual H<sub>3</sub>PO<sub>4</sub>, after extraction of CO<sub>2</sub> gas, was analysed for Ca, Mg, Sr, Fe and Mn (Coleman et al., 1989) using a Thermo Jarrell Ash-AtomScan 25 Inductively Coupled Plasma Source Spectrometer at the University of Ottawa. The chemical data were recalculated on an insoluble residue-free basis (100% soluble dolomite or calcite). The analytical precision and accuracy, in relative percent for each element, are the following Ca (2.1, 1.9), Mg (5.5, 0.4), Sr (2.7, 0.2), Fe (2.1, 0.3), and Mn (1.4, 2.9), respectively.

Guided by the carbon and oxygen isotope results and by petrographic observations, some samples were selected for Sr-isotope analysis. About 5 mg of the powdered sample was dissolved in 2.5 N ultrapure HCl and, after evaporation, Sr was extracted with quartz glass exchange columns filled with Bio Rad AG50WX8 ion exchange resin. Finally, ~75–100 ng Sr was loaded on Re filaments using a Ta<sub>2</sub>O<sub>5</sub>–HNO<sub>3</sub>–HF–H<sub>3</sub>PO<sub>4</sub> solution. Measurements were performed with a Finnigan MAT 262 multicollector mass spectrometer at the Institut für Geologie, Mineralogie und Geophysik, Ruhr Universität, Bochum, Germany (cf. Diener et al., 1996; Azmy et al., 1999).

Two standard reference materials were utilized as quality control of Sr isotope ratio measurements, NIST (NBS) 987 and USGS EN-1. The latter, representing modern sea water and treated like an ordinary sample, gave a <sup>87</sup>Sr/<sup>86</sup>Sr value of 0.709151 with a ( $2\sigma$ ) precision, calculated from seven measurements, of  $\pm 0.000008$ . About 75 ng Sr of the NIST (NBS) 987 standard reference material was directly loaded onto the filament and these results therefore represent only the internal reproducibility of mass-spectrometry. Its value was  $0.710236 \pm 0.000008$ , based on ten measurements. The average composite blank for Sr, including chemicals, ion-exchange columns and loading blank, did not exceed 0.0085 ng. The measured <sup>87</sup>Sr/<sup>86</sup>Sr ratio was normalized to a value of 8.375209 for the <sup>88</sup>Sr/<sup>86</sup>Sr ratio.

FORMATION	MEMBER	FACIES	CORE	LITHOLOGY	APPROX. THICKNESS (m)	
<b>V A Z A N T E</b>	<b>L A P A</b>	<b>PAMPLONA</b>	<b>CMM 279 KVD 60</b>		230	Dolomites, shale lenses, metamorphism.
						Banded dolomite microbial mats, pelloidal grainstones with frequent stromatolite interbeds, interparticle cavities filled with several generations of dolomite cements, extensive silicification
						Dolomitized microbial laminites, carbonate-rich shale interbedds at the top, columnar stromatolite lenses in the middle.
	<b>MORRO DO PINHEIRO</b>	<b>INFERIOR</b>	<b>CMM 500</b>	350	Shales with frequent dolomitic microbial laminites in the base portion, peloidal grainstone (Fig. 3b), cavities are always filled with dolomite cement, minor silicification.	
		<b>SUPERIOR</b>	<b>CMM 244</b>	450	Microbial mat dolostones, bird-eye structures ( Fig. 3a) filled with dolomite cements, minor silicification, black shale lenses at the top.	
		<b>INFERIOR</b>	<b>CMM 244</b>	430	Fenestral banded microbial dolostones, dolomite cements that totally occlude fenestrae, frequent silicification, common stromatolite lenses in the lower part.	
	<b>SERRA DO GARROTE</b>					Slates and graywackes, limestone interbeds

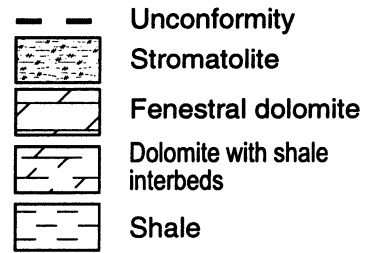


Fig. 2. Lithostratigraphy of the Vazante Formation with stratigraphic range covered by each core (De Oliveira, 1998, pers. comm.).

The sulfur isotope analyses were run on trace sulfate trapped in carbonates, following the method of Hall et al. (1988), at the Environmental Isotope Laboratory of the University of Waterloo, Ontario, Canada. The S-isotope ratio was measured using a continuous flow mass spectrometer (MICROMASS) coupled to the Carlo Erba Elemental Analyser (CHNS-O) EA 1108. Results are reported in  $\delta$ -values as per mil relative to the Canyon Diablo Triolite Standard (CDT), with a precision of  $\pm 0.3\%$ .

## 5. Lithofacies and petrography of the Vazante Formation

The Vazante Formation represents a sequence of dolomitized shallow shelf sediments, mainly microbial mats and stromatolitic reefal lenses, interrupted by deposition of shales and by lenses of black shale. Vertical fractures, caused by tectonic deformation, are frequent and filled with late dolomite cement.

The stratigraphy of the Vazante Formation (Fig. 2) has been refined by several authors (Madalosso, 1979; Rigobello et al., 1988; Freitas-Silva and Dardenne, 1992; Hitzman and Fogarty, 1997; Dardenne et al., 1998). The formation rests conformably on the non-carbonate deposits (slates and graywackes) of the Serra do Garrote Formation and is unconformably overlain by the dolostone deposits of the Lapa Formation. The thickness of the units varies laterally and depends therefore on borehole location. The dominant component is microbial lime mud deposited in inter- to supratidal environment that has been completely dolomitized during an early stage of diagenesis. This is indicated by stylolites that crosscut the pervasive dolomite, the earliest phase that selectively affected microbial carbonate mud matrix. Fig. 2 summarizes the composite petrographic profile, as discussed in detail in Rigobello et al. (1988) and De Oliveira (1998), person. comm.).

The diagenetic history of the Vazante Formation shows that it has been affected by multiple episodes of dolomitization, mechanical and chemical compaction, silicification and minor sideri-

tization and anhydritization that might have occurred in shallow, intermediate and deep burial environments (Dardenne, 1979; Madalosso, 1979). This study focuses solely on the major dolomitization processes, since all carbonate rocks in the studied cores were entirely dolomitized. Based on petrography and CL, four major phases of dolomitization have been recognized. These phases, from the oldest to the youngest, are: Dolomite I (pervasive dolomite), Dolomite II (replacement of fibrous cement), Dolomite III (equant cement) and Dolomite IV (latest equant and fracture-filling saddle cement).

### 5.1. Dolomite I

Dolomite I (Fig. 4a) is the most abundant type ( $\geq 80\%$  by volume) and it consists of inclusion-rich pervasive xenotopic dolomite (cf. Sibley and Gregg, 1987). It is non luminescent to dull or having sometimes medium CL (Fig. 4b). The dolomite I is a mimetic, fabric-preserving dolomite (cf. Fairchild, 1991; Budd, 1997) with crystal size varying between micrite and microsparite. The crystal size depends on the precursor texture. Increase in crystal size, however, has not been clearly associated with dolomitization. Inclusions in dolomites are usually relicts from their precursor carbonates (Sibley, 1982; Dawans and Swart, 1988; Budd, 1997), but those in the Vazante dolomites are mostly clays. Pervasive dolomitization affected mainly microbialites (microbial aggregates) and carbonate mud matrix (cf. Fairchild, 1991) and probably happened at an early stage of burial, since it is crosscut by stylolites (cf. Choquette and James, 1987). The retention of fabric, and near-micritic crystal size, all indicate that the original sediment did not suffer from extensive and/or repeated meteoric alteration. Fabric-destructive pervasive dolomites have been observed only sporadically in the core CMM 279 where they exhibit a brighter CL.

### 5.2. Dolomite II

Dolomite II consists of inclusion-rich fibrous crystals (Fig. 4a) that likely replaced the precursor marine calcite cements (e.g. Fairchild, 1991;

Fairchild et al., 1991). It is present in two sub-phases, A and B. The subphase A is represented by dolomite that replaced an early generation of fibrous cements and is characterized by small fibrous crystals (0.06–0.4 mm) that exhibit dull CL (Fig. 4b). The subphase B consists of dolomite that replaced a later generation of fibrous cements. The crystals of this subphase are usually larger than those of the early generation (0.6–2.4 mm), their rims are clear at the top, and they exhibit zoned CL (Fig. 4b). By volume (~5%), fibrous cements are the least abundant phase.

### 5.3. Dolomite III

Dolomite III consists of a later stage pore-filling coarse equant crystals (0.15–1 mm) that are generally clear under plane polarized light (Fig. 4a), but zoned under luminescence (Fig. 4b). This type of cement is more frequent than the fibrous cement (~8% by volume) and consists of sub- to anhedral crystals with frequent overgrowths. This dolomite also contains fluid inclusions and it is suggested to have been formed at shallow to intermediate burial depth since it is cut by stylolites of late generations.

### 5.4. Dolomite IV

Dolomite IV, the latest cement generation, occludes previously uncemented pores and late vertical fractures (e.g. Fairchild and Spiro, 1987) and is believed to have been formed under deep burial conditions. It consists of very coarse subhedral crystals (0.8–3 mm) which commonly have a recognizable milky appearance in polished thin sections and slabs. The crystals may contain fluid inclusions and usually exhibit undulose extinction typical of saddle dolomite, but they are entirely non luminescent. In rare cases, they engulf bright red luminescent ghosts of equant cements that they might have replaced (e.g. Fairchild et al., 1991).

The complete occlusion of all pores and fractures reflects a continuous extensive late-stage cementation by the dolomitizing fluids that may have resulted in significant porosity reduction relative to the precursor. These dolomite generations

are common in all studied facies, with the exception of the xenotopic pervasive dolomite that is restricted to stromatolites and microbial carbonate muds.

In summary, morphologically the Dolomites I–III resemble Phanerozoic CaCO<sub>3</sub> cements (e.g. Lohman and Walker, 1989; Al-Aasm and Lu, 1994; Al-Aasm and Azmy, 1996; Wenzel, 2000). The petrographic characteristics of generations I and II mimic a marine precursor cement, whereas the generation III resembles cement of shallow to intermediate burial stages. CL images, although clearly distinct for all three types, often show zoning, indicating that dolomitization progressed in pulses, and from solutions that were not chemically identical. This and the retention of original textural features (Fig. 3b) favour, in our view, a diagenetic origin for these dolomites as opposed to direct precipitation from Proterozoic seawater. Deposition of fibrous dolomite cements directly from seawater was not yet described in literature, either for ancient or modern carbonates (Tucker and Wright, 1990), and kinetic and thermodynamic models of experimental dolomite precipitation also indicate that fibrous dolomite is unlikely to precipitate directly from solutions (Tucker and Wright, 1990; Arvidson and Mackenzie, 1997, 1999). Although the issue of primary vs. diagenetic origin of Precambrian dolostones is still an open one, it is these considerations as well as the later discussed chemical and isotopic constraints that lead us to favour the diagenetic origin for the Vazante dolostones.

The last phase, Dolomite IV, is non-luminescent (Fig. 4b) and does not contain any replacement textures, suggesting that it likely sealed the remaining pores and fractures at late diagenetic stages.

## 6. Geochemistry

### 6.1. Major and trace elements

Table 1 summarizes the distribution of major and trace elements in the Vazante dolomites. In terms of trace elements, the successive dolomite generations show a progression, particularly in Fe



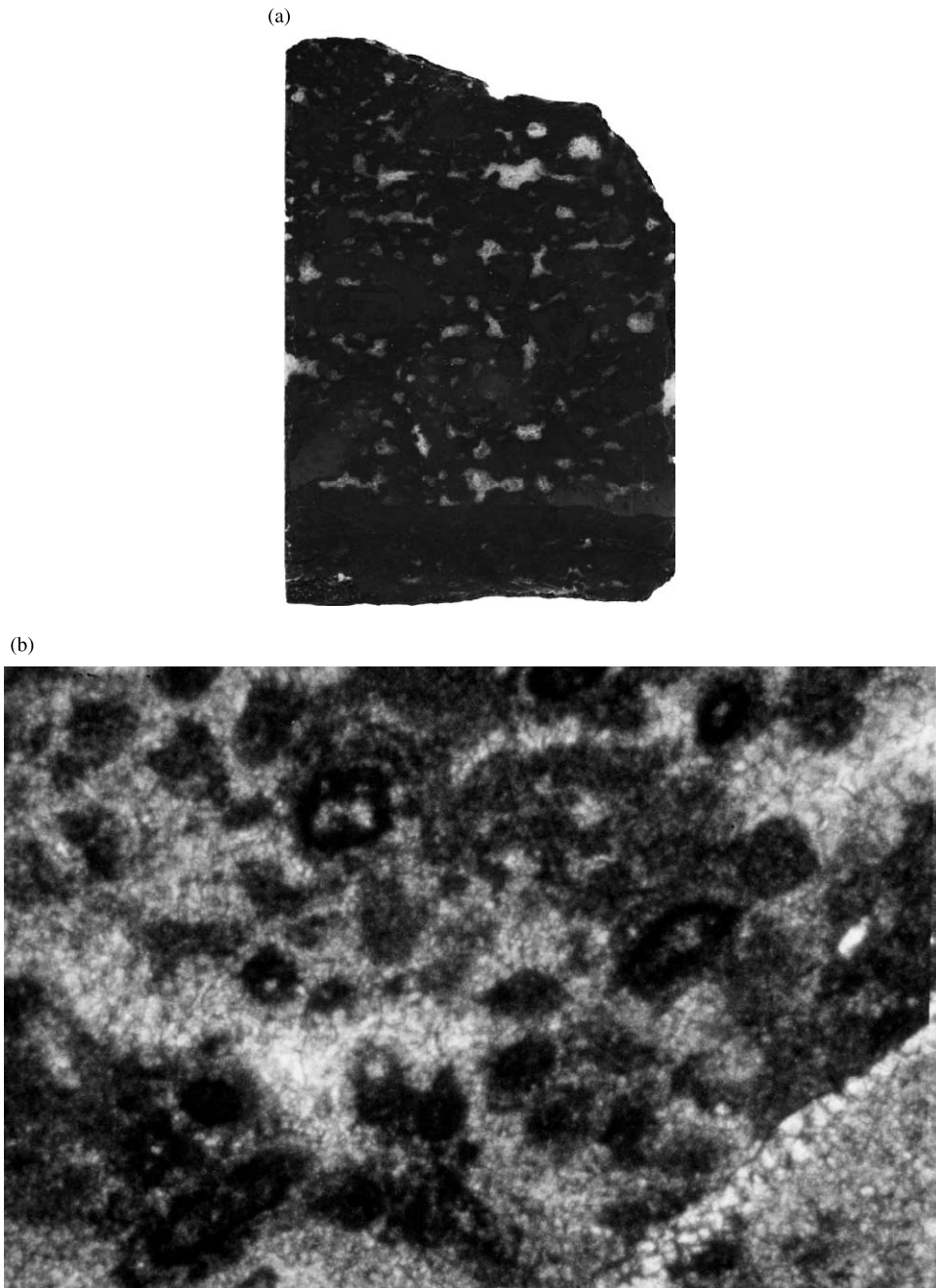


Fig. 3. Petrographic features from Core 244: (a) photograph of a polished slab (sample 244-45) showing fenestrae, filled with dolomite cement, in microbial mat facies. Field of view is 3.5 cm along *x*-axis, and (b) photomicrograph of a thin section (sample 244-29) with pelloidal grainstone fabric under plane polarized light. Field of view is 1.5 mm along *x*-axis.

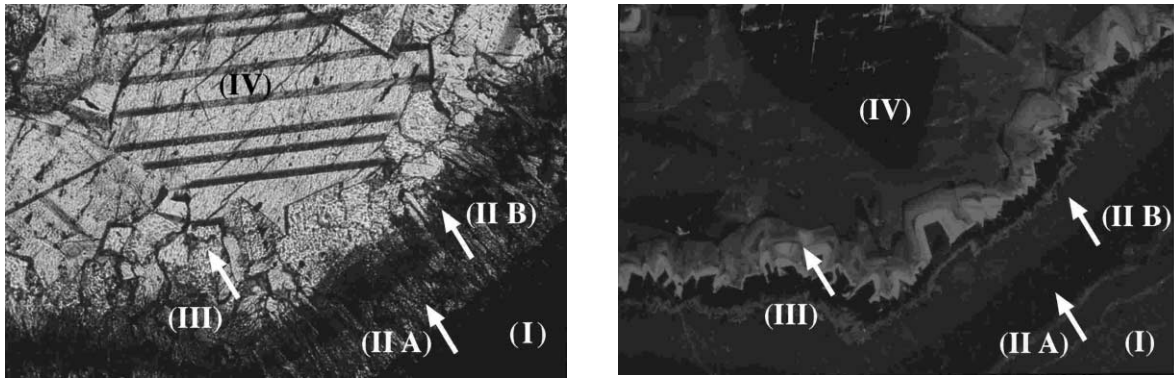


Fig. 4. Photomicrograph of a thin section (sample 244-42) with the successive (I–IV) dolomite generations: (a) fabric under plane polarized light; and (b) luminescence and zonation under luminescope. Field of view is 1.5 mm along x-axis.

and Mn contents (Fig. 5), although the overlap of values is considerable. In particular, the Dolomite IV contains significantly higher Mn and Fe concentrations than the Dolomite I–III varieties. In terms of major elements, Ca varies slightly from 52.7 to 57.9 mol%, as do their recent counterparts (cf. Budd, 1997). The dolomites are therefore mainly non-stoichiometric, with stoichiometry decreasing from Dolomite I–Dolomite IV.

Strontium concentrations can be utilized for understanding the nature of the dolomitizing fluid. Remnant inclusions of precursor carbonate (calcite or aragonite) and distribution coefficient of Sr ( $D_{sr}$ ) between dolomite and diagenetic fluids are generally the major factors controlling the Sr concentrations in dolomite (Budd, 1997). Because of the low Sr-contents (16–110 ppm; Appendix A), it is not likely that the Vazante dolomites contain remnant precursor inclusions, a statement supported by the XRD screening. The dolomites therefore reflect mostly the nature of the dolomitizing fluid. Estimates of Sr distribution coefficient ( $D_{sr}$ ) for dolomite vary from 0.015 to 0.06 (Veizer, 1983; Vahrenkamp and Stewart, 1990; Banner, 1995; Budd, 1997). If the Sr content were mainly due to  $D_{sr}$  and Sr/Ca of the dolomitizing fluid, the latter can be calculated from equation  $(Sr/Ca)_{dolomite} = D_{sr}(Sr/Ca)_{fluid}$ . Such calculations yield molar Sr/Ca for the Vazante dolomitizing fluid of 0.0023 to 0.0138 for  $D_{sr} = 0.015$ , and 0.0006–0.0035 for  $D_{sr} = 0.06$ . These values span the range from, to significantly less than, the Sr/Ca ratio of present-

day seawater (0.0086; Drever, 1988). Nonetheless, the average Sr concentrations are in the  $55 \pm 15$  ppm range (Table 1), suggesting that we are dealing with Sr-depleted dolomitizing fluids, likely due to partial or full meteoric water contributions. The considerable uncertainty in  $D_{sr}$  value of dolomite argues, nonetheless, for some caution in this interpretation.

Iron and Mn contents (Table 1), in contrast to Sr, reflect more the redox state of the diagenetic environment than the ionic strength of the dolomitizing fluid. The general trend (Fig. 5) of rising Fe and Mn concentrations from Dolomite I to Dolomite IV is a reflection of increasingly more reducing conditions with depth, particularly for the latter variety. The Vazante dolomites should still be considered as non-ferroan types, since their  $FeCO_3$  contents are less than 2 mol% (Tucker and Wright, 1990). Only some of the Dolomite IV (the latest cements) may have significantly higher Fe-concentrations ( $Fe \geq 11\,400$  ppm).

In summary, the major and trace element contents (Ca, Mg, Sr, Mn, and Fe) of Vazante dolomites (Table 1) are within the ranges observed for their recent counterparts (cf. Fairchild and Spiro, 1987, 1990; Fairchild, 1991; Budd, 1997).

## 6.2. Oxygen and carbon isotopes

Dolomitization of carbonates needs large volumes of water, in order to supply the required Mg. As a result, oxygen isotopic composition of a

dolomite product mostly reflects the isotopic composition of the dolomitizing water (Land, 1992). The  $\delta^{18}\text{O}$  and  $\delta^{13}\text{C}$  values of the Vazante dolomites (Table 1) range from  $-14.3$  to  $-0.1\text{‰}$  and  $-2.3$  to  $3.9\text{‰}$  PDB, respectively (Fig. 6). There is no correlation between  $\delta^{18}\text{O}$  and  $\delta^{13}\text{C}$ , but the Dolomite IV (latest cements) is discernibly more depleted in  $^{18}\text{O}$  than the other three types. This dichotomy may have been caused mainly by temperature increase during progressive burial (cf. Lohmann, 1988), a proposition supported by the below discussed fluid inclusion data.

The  $\delta^{18}\text{O}$  of dolomitizing fluid can be estimated, providing that its temperature is established by other means, such as homogenization ( $T_h$ ) and melting ( $T_{m,ice}$ ) temperatures of primary fluid inclusions. Unfortunately, in our case, the inclusions were so small that  $T_h$  were measured only in the two-phase inclusions. This precludes an estimate of salinity for the dolomitizing fluid as well as application of pressure correction. The all-liquid inclusions trapped in Dolomites II and III (fibrous and early equant cements) indicate that dolomitization commenced during early stages of diagenesis at temperature below about  $50\text{ °C}$  (cf. Goldstein and Reynolds, 1994), pre-

sumably at near-surface temperature of about  $30\text{ °C}$ . The mean homogenization temperatures (Table 2) of the two-phase inclusions trapped in Dolomite IV (the latest pore- and fracture-filling saddle dolomite cement), on the other hand, indicate that it was formed at temperature of at least  $120\text{--}130\text{ °C}$  (cf. Goldstein and Reynolds, 1994), hence during later stages of burial. The latter temperature estimates would suggest depth of several km, up to  $6.7\text{ km}$  if a geothermal gradient of  $15\text{ °C/km}$  is applied (Ussami, 1993). Some of the fracture-filling Dolomites IV contain also one phase all-liquid inclusions. These probably developed as a consequence of sudden release of lithostatic pressure due to uplift and erosion. Accepting the above temperature constraints, the  $\delta^{18}\text{O}$  values of the dolomitizing fluid for Dolomites I–III was likely within the  $-8$  to  $-3\text{‰}$  and for Dolomite IV from  $+2$  to  $+6\text{‰}$  SMOW (Fig. 7).

Paleomagnetic data for Precambrian rocks enable differing plate reconstructions (Hoffman, 1991; Meert and Van der Voo, 1994; Li et al., 1995; Park et al., 1995; Schmidt and Williams, 1995; Torsvik et al., 1996; Ross, 1999) for the

Table 1  
Ca, Mg, Fe, Mn, Sr,  $\delta^{18}\text{O}$  and  $\delta^{13}\text{C}$  statistics for the Vazante dolomites

Generation		CaCO <sub>3</sub> (%)	MgCO <sub>3</sub> (%)	Sr (ppm)	Fe (ppm)	Mn (ppm)	$\delta^{18}\text{O}$	$\delta^{13}\text{C}$	$^{87}\text{Sr}/^{86}\text{Sr}$
Dolomite I	<i>n</i>	45	45	45	45	45	45	45	35
	Max.	57.9	47.3	106	14 492	392	-0.1	3.9	0.731601
	Min.	52.7	42.1	16	866	19	-10.3	-2.3	0.707247
	Mean	55.5	44.5	48	3160	155	-5.1	1.5	0.712592
	S.D.	1.1	1.1	18	2786	108	1.9	1.1	0.005739
Dolomite II	<i>n</i>	11	11	11	11	11	11	11	2
	Max.	57.4	44.6	58	7912	529	-1.8	2.6	0.710575
	Min.	55.4	42.6	36	530	82	-6.3	1.4	0.706144
	Mean	56.2	43.8	44	2773	273	-4.5	1.9	0.708360
	S.D.	0.7	0.7	8	2386	173	1.4	0.4	0.003133
Dolomite II	<i>n</i>	4	4	4	4	4	4	4	1
	Max.	56.8	45.0	83	7564	879	-5.2	2.1	0.715374
	Min.	55.0	43.2	57	3326	642	-6.4	1.6	0.715374
	Mean	56.0	44.0	68	5885	736	-5.6	1.7	0.715374
	S.D.	0.7	0.7	13	2015	103	0.6	0.2	
Dolomite I	<i>n</i>	16	16	16	16	16	16	16	8
	Max.	57.8	45.4	110	22 009	2094	-7.8	3.3	0.725232
	Min.	54.6	42.2	18	1942	137	-14.3	0.2	0.708526
	Mean	56.5	43.5	40	9919	697	-9.8	1.5	0.713219
	S.D.	0.9	0.9	24	5661	496	1.6	0.7	0.005668

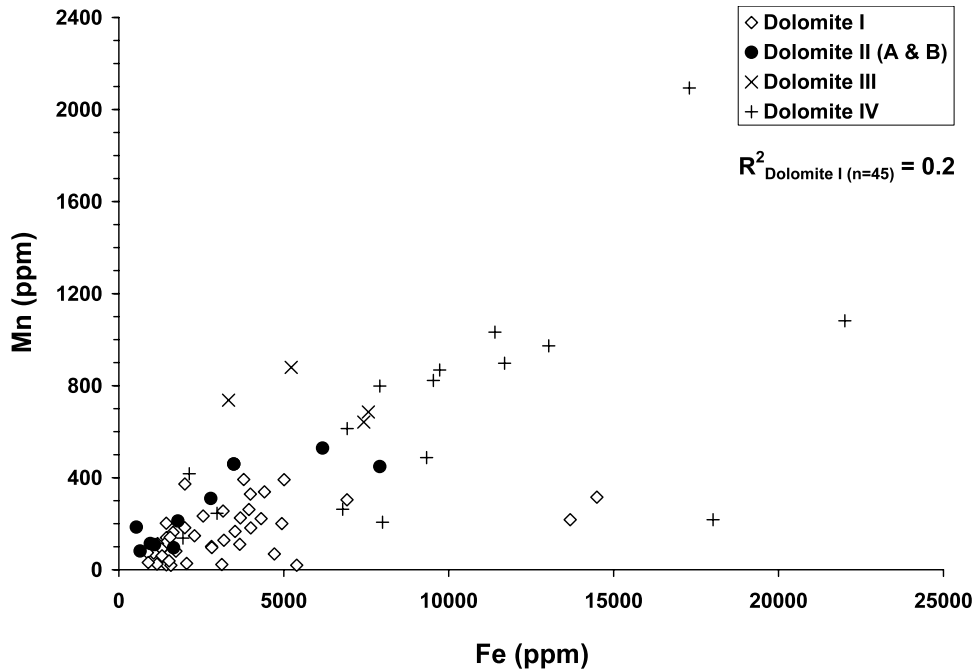


Fig. 5. Scatter diagram of Fe vs. Mn for different dolomite generations of the Vazante Formation.

Amazonia plate, including its Vazante area. Nevertheless, the abundance of microbial mats with fenestral fabrics (cf. Pratt et al., 1992) and thick stromatolite beds, and minor evaporite occurrences (see below), in the carbonate sequences indicate warm conditions and low latitude paleolocation. In similar modern environments, the  $\delta^{18}\text{O}$  of seawater is  $\sim 0\text{‰}$  SMOW and that of meteoric water is lower by about  $4\text{‰}$  (Clark and Fritz, 1997). Assuming that the  $\delta^{18}\text{O}$  values of the Vazante-times seawater and of meteoric waters were similar to those of today, the  $\delta^{18}\text{O}$  of  $-8$  to  $-3\text{‰}$  SMOW for the Dolomite I–III fluids would imply that dolomitizing solutions were almost entirely of a meteoric type. This, however, would create a problem with the source of Mg (Land, 1992).

It is, on the other hand, possible that  $\delta^{18}\text{O}$  of past seawater differed from the present day one, being shifted to  $^{18}\text{O}$  depleted values (Veizer et al., 1999). The histogram of  $\delta^{18}\text{O}$  for late Proterozoic carbonates (Fig. 8) shows, as for their Phanerozoic counterparts, that dolostones are similar to, or up to  $5\text{‰}$  heavier than, coeval limestones. The

overall pattern is, nevertheless, shifted to a more negative range, as would be expected if coeval seawater were depleted in  $^{18}\text{O}$  relative to its modern counterpart. Considering the uncertainty in the value of dolomite–calcite, and dolomite–water, fractionation factors (Land, 1983; Budd, 1997), we shall utilize the limestone values in attempt to constrain the  $\delta^{18}\text{O}$  of coeval seawater. These show a mode of about  $-6\text{‰}$  PDB (Fig. 8) which is simultaneously the heaviest, hence the ‘best preserved’, signal. In the Phanerozoic, diagenetic stabilization usually leads to  $\sim 2\text{‰}$  depletion in the whole rock signal (Fig. 20 in Veizer et al., 1999). Assuming a comparable shift for the Proterozoic limestones, the coeval tropical seawater could have had  $\delta^{18}\text{O}$  of about  $-4\text{‰}$  SMOW. This is close to the upper limit of estimates for Dolomites I–III (Fig. 7). Consequently, the suggested range of  $-3$  to  $-8\text{‰}$  SMOW for fluids generating the Dolomites I–III would be consistent with their origin from early diagenetic solutions that were generated by mixtures of sea and meteoric waters. Their chemical attributes are also in agreement with this proposition.

The petrological, fluid inclusions and chemical considerations for Dolomite IV, on the other hand, convincingly suggest that it is a product of deep burial. The parental fluids were therefore likely evolved formation waters enriched in  $^{18}\text{O}$ . This could explain the calculated  $\delta^{18}\text{O}_{\text{fluid}}$  of +2 to +6‰ SMOW (Fig. 7).

The overwhelmingly positive  $\delta^{13}\text{C}$  (Fig. 6) likely reflect the carbon isotope composition of the precursor carbonate, due to relatively low  $\text{CO}_2$  content of diagenetic waters (Land, 1992). The few  $^{13}\text{C}$  depleted values, from microbial aggregates and carbonate muds, occur at the top of the formation (Appendix A, Fig. 2) and are probably stratigraphically controlled, since the trend is reflected in both, microbial laminites and non-microbial (fibrous cements) components (Fig. 6; Appendix A).

In summary, petrographic, fluid inclusion, chemical criteria and stable isotopes of the Vazante carbonates reflect two major dolomitization events: (1) an early episode that affected microbial laminites and fibrous and early equant cements (Dolomite I, II and III); and (2) a late episode

that deposited the latest pore- and fracture-filling (saddle) dolomite cements (Dolomite IV) in deep burial settings.

We do not consider evaporitic sabkha-type dolomitization to be applicable to the Vazante Dolomites I–III. Unlike sabkha dolostones, the Vazante Formation in the studied cores does not contain any evaporite interlayers. In the São Francisco Basin, few gypsum nodules and thin laminae have been observed only in the Paracatu (Morro Agudo) area (Madalosso, 1979) and in the adjacent basins (e.g. the Salitre Formation of the Una Group; Misi and Kyle, 1994; Misi and Veizer, 1998). Furthermore, the low Sr contents and the  $\delta^{18}\text{O}$  of the studied dolomites are also difficult to reconcile with their being a product of concentrated evaporitic brines.

## 7. Isotope stratigraphy

The retention of some original isotope signal is possible only in well preserved samples. A plethora of techniques and tests was proposed for

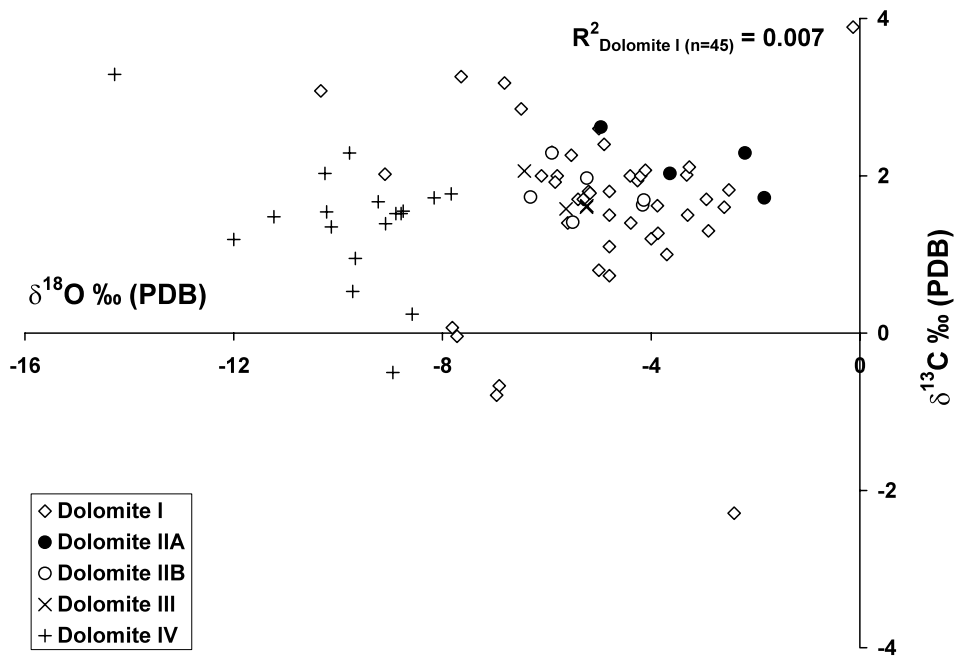


Fig. 6. Oxygen vs. carbon isotope values for the Vazante dolomite generations.

Table 2

Statistical data for homogenization temperatures measured in fluid inclusions of Dolomite IV

Sample I	244-26	244-45	244-57	244-78	244-80	Total
Dolomite g	IV	IV	IV	IV	IV	IV
No. me	1	23	16	32	8	60
Mean Th	118	132	130	124	116	127
Maximum		157	167	145	127	157
Minimum		116	118	108	103	103
S.D.		15	15	8	11	17

evaluating the degree of sample preservation (cf. Veizer, 1983; Fairchild and Spiro, 1987; Kaufman et al., 1991, 1992, 1993; Derry et al., 1992; Narbonne et al., 1994), none yielding unequivocal results, but giving reasonable estimates of sample quality if applied in combination. In the subsequent text we shall focus on microbial mud and microbial aggregates and on few available early fibrous cement components, since these are the most likely phases to retain their near-primary seawater signals, at least for some isotopes.

Chemical composition of rocks is a reflection of their diagenetic history. In the course of diagenesis, some elements, such as Mn and Fe, are enriched in the successor phase while others, such as Sr and Na, are depleted (Brand and Veizer, 1980; Veizer, 1983). The Mn/Sr value has been, therefore, used as a first order indicator of the degree of preservation (e.g. Derry et al., 1992). Usually, only samples with Mn/Sr ratio of  $< 3$  are taken as 'well preserved' from the point of view of isotope proxies (Derry et al., 1992; Kaufman et al., 1992, 1993; Kaufman and Knoll, 1995). Nonetheless, cases do exist where samples with Mn/Sr ratio of up to 10 appear to yield reasonable isotope signals (Narbonne et al., 1994), while samples with very low Mn/Sr ratio may not do so.

The preservation of an isotope signal in the successor phase depends on the water/rock ratio (Banner and Hanson, 1990) for a given element at the time of diagenetic recrystallization. The usual sequence for water/rock ratio is  $O > Sr > C$  (cf. Jacobsen and Kaufman, 1999). Thus the preservation of C-isotope signal is possible even with high degree of recrystallization, while O isotopes will mostly be reset. Note, however, that in contrast to the model of Banner and Hanson (1990) and

Jacobsen and Kaufman (1999), we do not believe that the entire rock undergoes recrystallization with every batch of new water entering the sedimentary pile. Such a model demands some  $10^4$  batches of water, and bulk recrystallization events, and would result in complete loss of textures and in homogenization of the chemical and isotope signals. This, quite clearly, is not the case for most carbonate rocks. Instead, recrystallization is considered to be a localized phenomenon (Brand and Veizer, 1980; Maliva, 1998; Veizer et al., 1999), with only few recrystallization steps. This permits localized preservation of mineralogy, textures and chemistry and of the internal heterogeneity of the rock.

The Vazante Dolomites I–III have Mn/Sr ratios from 0.3 to 8.5 (Appendix A), many satisfying the above selection criterion. Note also that these are ratios for dolomites that, on crystallographic grounds, contain higher Mn and lower Sr contents than calcites and that there is no correlation between Sr and Mn (Fig. 9) or  $\delta^{18}O$  and Sr/Mn ratio (Fig. 10).

### 7.1. Carbon isotope profile

Based on the above discussion, the carbon isotope signal has the best potential for preservation of near-original values. The distribution of  $\delta^{13}C$  in Vazante samples (Fig. 10) has a mode at  $\sim 2 \pm 1\%$ , but also contains some negative values. The latter can be either a reflection of stratigraphic variations or of alteration phenomena.

Post-depositional shifts in  $\delta^{13}C$  values for Proterozoic carbonates were observed (Knoll et al., 1986; Fairchild et al., 1990; Kaufman et al., 1992; Narbonne et al., 1994), but most whole-

rock samples, more as a rule than an exception, retain their carbon isotope composition (Fairchild and Spiro, 1987; Burdett et al., 1990; Kaufman et al., 1991). This appears to hold even for dolomitization processes, because dolomitization (and diagenetic) fluids generally have low carbon contents. Even in cases of severe alterations, the shifts are rarely more than  $\sim 2\text{‰}$  (Sheppard and Schwarz, 1970). Metamorphic decarbonation of carbonate rocks in the presence of silicates could release isotopically heavy  $\text{CO}_2$ , thus lowering the  $\delta^{13}\text{C}$  values of the remaining carbonates (Shieh and Taylor, 1969), but the tectonic history and petrographic criteria for the Vazante rocks preclude the establishment of P/T conditions required for decarbonation (Madalosso, 1979; Rigobello et al., 1988). In the absence of decarbonation, even metamorphosed carbonates, such as marbles, tend to retain their near-original  $\delta^{13}\text{C}$  values (Wickham and Peter, 1993). We therefore conclude that the observed  $\delta^{13}\text{C}$  temporal trend (Fig. 11) mimics the original pattern, a conclusion in accord with the previous observation that various dolomite phases reflect the same pattern. If

so, what could be the causes of this stratigraphic trend?

Vital effects could influence isotopic fractionation of carbon, but no significant fractionation has been demonstrated from studies of Proterozoic stromatolites and associated muds (Fairchild, 1991). In another alternative, high photosynthetic rates in local basins may deplete the water column in  $^{12}\text{C}$ , or influx of  $\text{CO}_2$  from oxidation of organic matter may enrich it in  $^{12}\text{C}$ . Bacterial sulfate reduction and methanogenesis can cause comparable C isotope shifts (Schidlowski et al., 1983). Nevertheless, in our view, the low contents of organic carbon and low porosity of Vazante dolomites do not support the scenarios that would invoke large primary productivity or large role for the oxidized organic matter.

The  $\delta^{13}\text{C}$  pattern of the Vazante Formation (Fig. 11) consists of two major parts. The lower portion is characterized by a generally smooth signal that commences with  $\sim 4\text{‰}$  (PDB) at the base and continues upsection with values at  $\sim 2\text{‰}$  to the base of the Fácies Médio of the Pamplona Member. The upper part, on the other

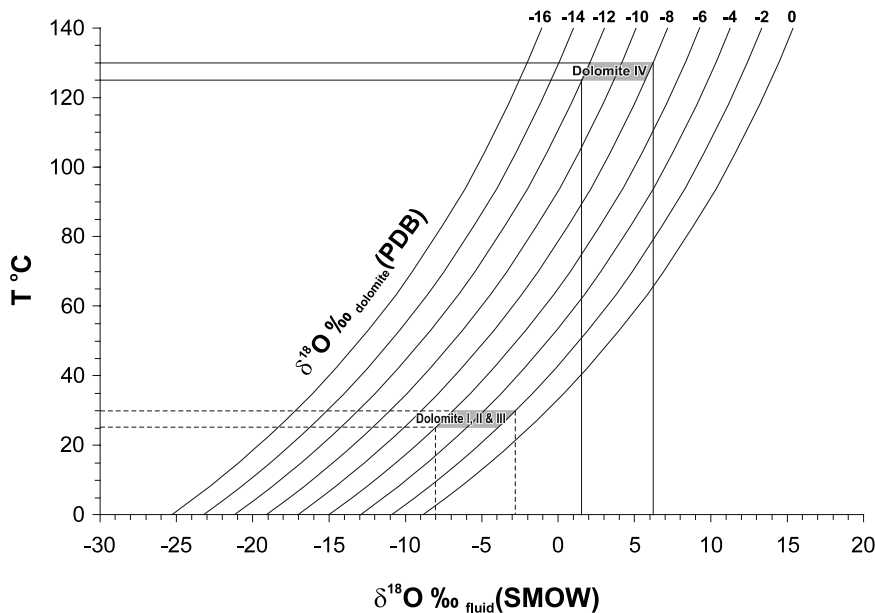


Fig. 7. Temperature vs.  $\delta^{18}\text{O}_{\text{diagenetic fluid}}$  for various  $\delta^{18}\text{O}_{\text{dolomite}}$  values that were reconstructed from the equation  $10^3 \ln \alpha = 3.2 \times 10^2 T^{-2} - 3.3$  (Land, 1983). The vertical bars indicate the ranges for  $\delta^{18}\text{O}_{\text{fluid}}$  based on the most enriched and depleted sample of a cluster for the given dolomite generation (Fig. 6). The shaded areas mark the preferred temperature ranges.

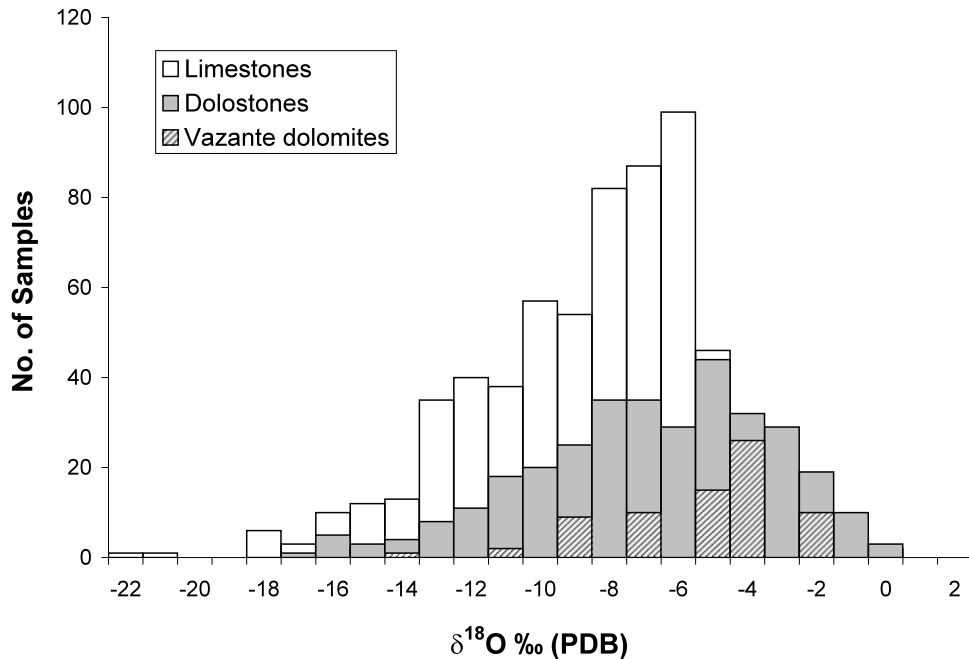


Fig. 8. Histogram of  $\delta^{18}\text{O}$  distribution for late Proterozoic carbonate sequences from different localities. Data were compiled from Kaufman et al. (1991, 1993), Derry et al. (1992, 1994), Corsetti and Kaufman (1994), Misi and Kyle (1994), Narbonne et al. (1994), Iyer et al. (1995), Bose et al. (1996), Pelechaty et al. (1996), Sarkar et al. (1998), McKirdy et al. (2001), and Fairchild et al. (2001). Dolomites associated with glaciogenic sequences, often having  $^{18}\text{O}$  enriched signal are excluded from the histogram.

hand, shows a strongly oscillating signal with two large negative shifts, of about  $-4\text{‰}$ , at the top of the *Fácies Médio* and in the *Fácies Superior*. The  $\delta^{13}\text{C}$  of the overlying Lapa Formation, above an unconformity, also continues with the negative values.

If the hypothesis of Kaufman et al. (1991, 1993), Kaufman and Knoll (1995), Kaufman et al. (1997), equating large negative  $\delta^{13}\text{C}$  shifts with glacial phases, is substantiated, a proposition that requires verification by data with better temporal resolution than presently available, then the two negative  $\delta^{13}\text{C}$  spikes at Vazante may have a similar cause and the sequence would likely be of Neoproterozoic age. The Neoproterozoic is believed to have had two major global glacial phases (Fig. 12), the late Sturtian one at the base of the Neoproterozoic and the Varanger one in the upper Neoproterozoic (Knoll et al., 1986; Fairchild and Spiro, 1987; Derry et al., 1989, 1992; Kaufman and Knoll, 1995; Narbonne and Aitken, 1995; Kaufman et al., 1997; Saylor et al., 1998;

Jacobsen and Kaufman, 1999; Walter et al., 2000).

Similar negative  $\delta^{13}\text{C}$  plunges were documented also in the isotope pattern of the Bambuí carbonates (Iyer et al., 1995; Kawashita, 1998; Misi and Veizer, 1998) but these rocks, in contrast to Vazante, rarely contain *Conophyton*, the latter being more abundant in the Mesoproterozoic carbonates. Accepting the proposition that the glaciation/low  $\delta^{13}\text{C}$  association is universally valid for the Neoproterozoic, the negative  $\delta^{13}\text{C}$  signals in the Vazante Formation could be correlated either with the Sturtian or the Varanger glaciations (Figs. 11 and 12) but the abundant *Conophyton* favours more the former alternative.

## 7.2. Strontium isotope profile

A detailed temporal variation in strontium isotopic signals of Phanerozoic seawater, based on low-Mg calcite shells, was recently published by Veizer et al. (1999) and utilized for age estimates



at a high level of resolution (Azmy et al., 1999). In the Precambrian, the task is more onerous because these carbonates were affected by diagenetic stabilization processes that modify the encrypted primary isotope signal. Furthermore, the Neoproterozoic seawater  $^{87}\text{Sr}/^{86}\text{Sr}$  trend is not well established, mostly due to uncertainties of geochronology. Nevertheless, due to the relatively good preservation of some Proterozoic carbonates and due to the fact that Sr-isotope signal in diagenetic solutions is often buffered by the dissolving precursor phase (Veizer and Compston, 1976; Veizer, 1983; Derry et al., 1989; Kaufman et al., 1993; Banner, 1995; Kaufman et al., 1997; Jacobsen and Kaufman, 1999), a preliminary delineation of  $^{87}\text{Sr}/^{86}\text{Sr}$  for Neoproterozoic seawater does exist (Fig. 12).

In general, the Vazante  $^{87}\text{Sr}/^{86}\text{Sr}$  values decline with increasing Sr contents (Fig. 13), clearly reflecting contamination by radiogenic Sr from silicate phases. Consequently, only the least radiogenic samples can perhaps be regarded as the ‘best

approximation’ of contemporary seawater (Veizer and Compston, 1976). For the Vazante, these are 0.70724–0.70734 from microbial aggregates and carbonate mud and 0.70614 from a fibrous cement (Figs. 11–13 and Appendix A). The underlying Serra do Garrote limestones have  $^{87}\text{Sr}/^{86}\text{Sr}$  value of 0.70690 and the overlying Lapa microbial aggregates 0.70684 (Appendix A). Except for the fibrous cement, the remaining ‘best’ estimates seem to be compatible with either the Sturtian or the Varanger values (Derry et al., 1989; Kaufman et al., 1993; Gorkhov et al., 1995; Kaufman et al., 1997; Jacobsen and Kaufman, 1999), but they all clearly precede the steep rise in  $^{87}\text{Sr}/^{86}\text{Sr}$  in the terminal Proterozoic (Fig. 12). Should the fibrous cement be the best approximation for the original seawater value, a Sturtian age would again be preferred.

For comparison, the values from the latest cements (Dolomite IV) varied from 0.70853 to as high as 0.72523 (Fig. 13), reflecting the deep burial conditions of diagenetic fluids that have

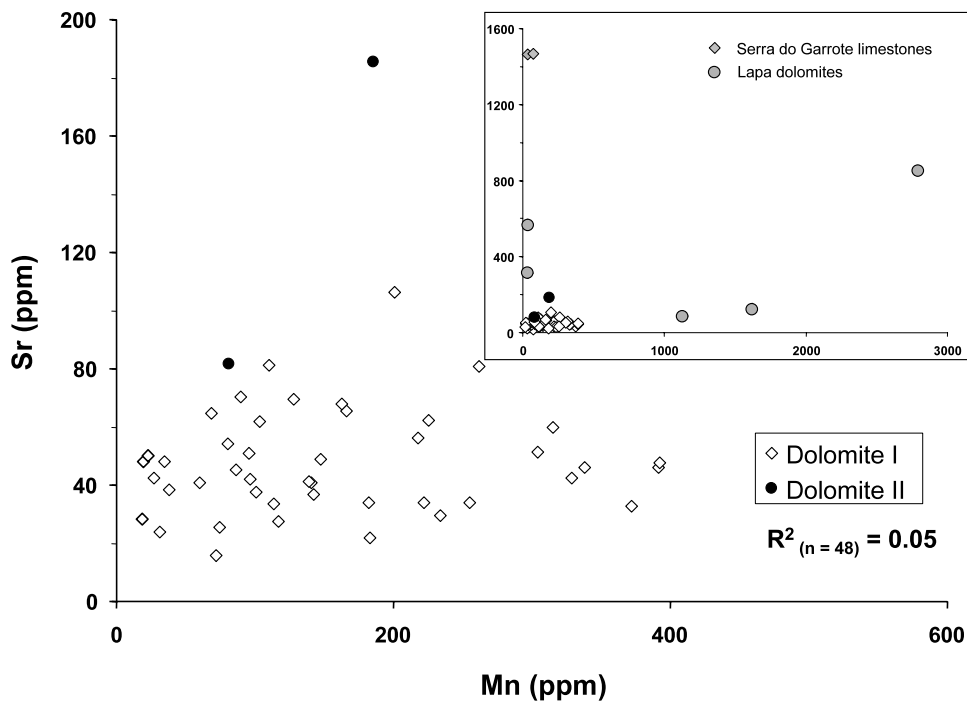


Fig. 9. Scatter diagram of Mn vs. Sr for the Vazante dolomites. Some samples are from the underlying Serra Do Garrote limestones and the overlying Lapa dolomites.

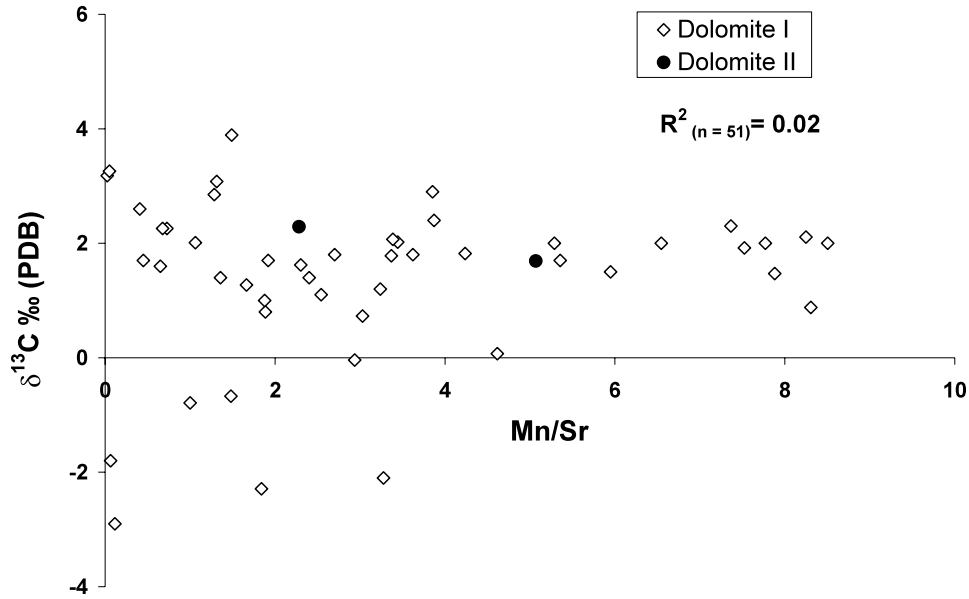


Fig. 10. Scatter diagram of  $\delta^{13}\text{C}$  vs. Mn/Sr for the same set of samples as in Fig. 9.

circulated through clastic rocks, such as shale beds within the basin.

### 7.3. Sulfur isotope profile

The variations in S-isotope composition of marine sedimentary sulfates through time (Strauss, 1993, 1997) can also be utilized for isotope stratigraphy. Several factors, discussed in detail in Strauss (1997), influence the  $\delta^{34}\text{S}$  signals of sedimentary evaporitic sulfates, the latter often reflecting local environmental conditions rather than open seawater. Trace sulfates incorporated in carbonates may, at times, provide therefore a more representative  $\delta^{34}\text{S}$  signal for open seawater (cf. Claypool et al., 1980; Holser et al., 1988; Schidlowski, 1989). Due to fragmentary record, and to large uncertainty in the assigned radiometric ages, the Precambrian  $\delta^{34}\text{S}$  signal has a wide scatter around  $\sim 20\text{‰}$  mean, with an abrupt increase to  $\sim 30\text{‰}$  (Fig. 12) towards the Precambrian/Cambrian boundary (Claypool et al., 1980).

The scarcity of evaporite deposits in the Vazante sequence leaves the trace sulfates as the only available material that can provide the S-isotope signature. The  $\delta^{34}\text{S}$  of trace sulfate (mainly water

soluble) trapped in the Vazante carbonates (Fig. 11) varies between 16.9 and 10.8‰, while in the overlying Lapa Formation it reaches  $\sim 22\text{‰}$  (Appendix A). In order to confirm that the obtained isotope results do not reflect signals of oxidized sulfides, several samples were analyzed for total sulfur. These samples yielded comparable values to trace sulfate (Appendix A). Note that the high  $\delta^{34}\text{S}$  values, up to 31.7‰, reported by Iyer et al. (1992), originate from barites from the same basin, but from  $\sim 100$  km distant Paracatu area.

In conclusion, the relatively low Vazante  $\delta^{34}\text{S}$  signals suggests again stratigraphic position at around the Sturtian glaciation, in agreement with C- and Sr-isotope patterns.

## 8. Conclusions

Petrographic observations for the Proterozoic Vazante carbonates show that dolomitization of the precursor carbonates has been fabric retentive. This permits identification of four generations of dolomites: (1) Dolomite I (microbial mats); (2) Dolomite II (fibrous cements); (3) Dolomite III

(equant cement); and (4) Dolomite IV (late burial and fracture filling cement). Fluid inclusion studies suggest that dolomitization of Dolomite I–III commenced at temperatures below 50 °C, indicating that the process was already operative during an early diagenetic stage. Trace element chemistry and stable isotope data indicate that these dolimitizing fluids were a mixture of meteoric and sea waters, with  $\delta^{18}\text{O}$  estimated at about  $-3$  to  $-8\text{‰}$  (SMOW).

The isotope signals and trace element contents of the latest pore- and fracture-filling cements (Dolomite IV) suggest that they were formed under

deep burial conditions at temperature over 120 °C and at depth of several km.

Despite their extensive dolomitization, Vazante carbonates may still retain their inherited primary  $\delta^{13}\text{C}$  signature. Their C-isotope variations fluctuate slightly around 2‰ (PDB) through the lower part of the formation, followed by a significant negative plunge ( $\sim 4\text{‰}$ ) at the top (Fácies Superior, uppermost Pamplona Member). If this plunge is correlated with glaciation(s), a Neoproterozoic age is favoured for the Vazante sequence.

Unlike  $\delta^{13}\text{C}$  signal, the  $^{87}\text{Sr}/^{86}\text{Sr}$  signature is strongly altered, but samples with the lowest ratios

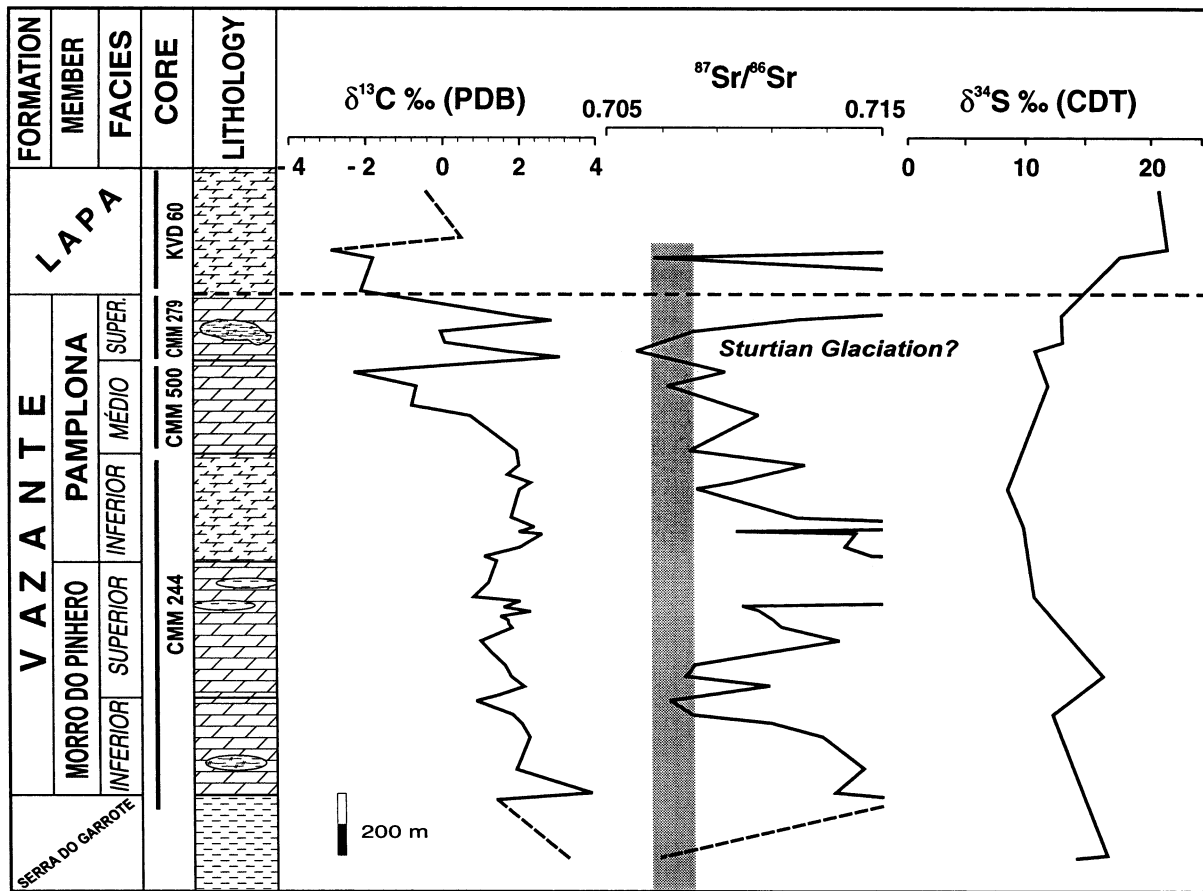


Fig. 11. Variations in  $\delta^{13}\text{C}$ ,  $^{87}\text{Sr}/^{86}\text{Sr}$  and  $\delta^{34}\text{S}$  for dolomites of the Vazante Formation. The shaded bar represents the range of the best preserved (lowest) global  $^{87}\text{Sr}/^{86}\text{Sr}$  signals for the Varanger and Sturtian glacial episodes (Fig. 12, and see also Jacobsen and Kaufman, 1999). Legend as in Fig. 2.

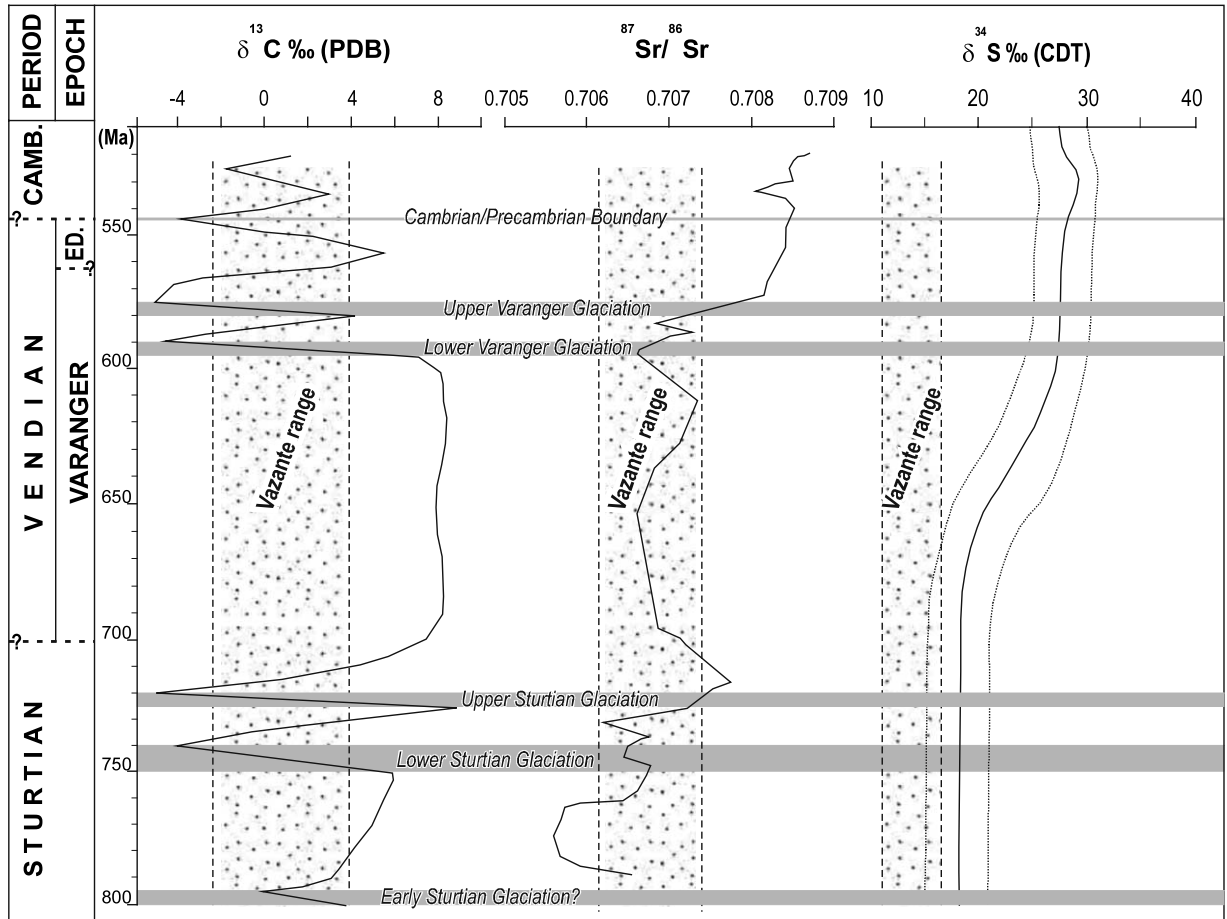


Fig. 12. Global trends for C-, Sr- and S-isotope variations during the Neoproterozoic (modified after Strauss, 1993; Jacobsen and Kaufman, 1999). The pattern is based on compilations from Derry et al. (1989, 1992, 1994), Asmerom et al. (1991), Strauss (1993), Kaufman and Knoll (1995), and Kaufman et al. (1993, 1996, 1997). The Sr isotope trend is an envelope around the least radiogenic values. The dashed lines represent the range of Vazante values. The assigned 'ages' are only approximations.

may have retained their near-primary values, ranging from 0.70614 to 0.70734, the former correlating approximately with the negative  $\delta^{13}\text{C}$  shift at the top of the formation. In agreement with the  $\delta^{13}\text{C}$  data,  $^{87}\text{Sr}/^{86}\text{Sr}$  and  $\delta^{34}\text{S}$  signals are also consistent with a Neoproterozoic age, possibly a Sturtian equivalent, for the Vazante Formation. Nevertheless, additional work is required to confirm this assertion since neither the background seawater trends nor the present data are unequivocal.

### Acknowledgements

The authors wish to thank I.J. Fairchild, N. James and A.J. Kaufman for reviews. This project was financed by the Natural Sciences and Engineering Research Council of Canada, the Financiadora de Estudos e Projetos-FINEP/PADCT grant no. 64.99.0264.00, Brazil, the Conselho Nacional de Desenvolvimento Científico e Tecnológico (CNPq, the National Research Council of Brazil), and the Cia Mineira de Metais, Vazante, Minas Gerais, Brazil.

**Appendix A. Samples, description, localities, stratigraphy, isotopic composition ( $\delta^{18}\text{O}$  and  $\delta^{13}\text{C}$  in ‰ PDB and  $\delta^{34}\text{S}$  in ‰ CDT) and trace element contents of the studied carbonates**

Field No.	Formatio	Member	Core	Dolomite	Depth (m)	$\delta^{18}\text{O}$	$\delta^{13}\text{C}$	$\delta^{34}\text{S}$	CaCO <sub>3</sub> %	MgCO <sub>3</sub> %	Mn(ppm)	Sr(ppm)	Fe(ppm)	<sup>87</sup> Sr/ <sup>86</sup> Sr	± 2σ	Mm/Sr	I/Sr
KV-60-1	Lapa		KVD-F60	I	284	-12.3	-2.9	22.0	87.54	12.46	36	314	21272	0.717515	0.000006	0.1	0.003
KV-60-3	Lapa		KVD-F60	I	310	-9.7	-1.8	18.0	90.77	9.23	37	570	2673	0.706841	0.000008	0.1	0.002
KV-60-4	Lapa		KVD-F60	I	416	-12.8	-2.1		97.32	2.68	2791	852	14141	0.730735	0.000009	3.3	0.001
KV-60-10	Lapa		KVD-F60	I	93	-7.7	-0.4	21.3	55.35	44.65	1621	127	11182	0.724166	0.000008	12.8	0.008
KV-60-12	Lapa		KVD-F60	I	244	-7.0	0.5		54.30	45.70	1130	87	8534	0.716869	0.000009	12.9	0.011
KV-279-1	Vazante	Pamplona	CMM-279	I	92	-6.5	2.9		55.09	44.91	90	70	1296	0.712034	0.000009	1.3	0.014
KV-279-1	Vazante	Pamplona	CMM-279	III	92	-8.8	1.5		56.32	43.68	245	27	2975			4.6	
KV-279-4	Vazante	Pamplona	CMM-279	I	165	-7.8	0.1	13.2	53.49	46.51	72	16	1052				0.024
KV-279-5	Vazante	Pamplona	CMM-279	I	193	-4.8	1.5		54.55	45.45	25	42	1157	0.708090	0.000007		0.027
KV-279-5	Vazante	Pamplona	CMM-279	II B	193	-4.1	1.7	10.8	56.33	43.67	185	37	530	0.706144	0.000009	5.1	
KV-279-8	Vazante	Pamplona	CMM-279	I	80	-9.1	2.0		52.72	47.28	141	41	1555			3.4	
KV-279-10	Vazante	Pamplona	CMM-279	I	129	-7.7	0.0		54.30	45.70	75	25	866	0.708213	0.000008	2.9	0.039
KV-279-11	Vazante	Pamplona	CMM-279	I	151	-7.7	-0.6		54.95	45.05	372	33	2001	0.711721	0.000009	1.3	0.030
KV-279-13	Vazante	Pamplona	CMM-279	I	212	-10.3	3.1		54.95	45.05	31	24	891				
KV-279-13	Vazante	Pamplona	CMM-279	IV	212	-14.3	3.3		55.35	44.65	137	18	1942	0.708623	0.000008		0.054
KV-500-1	Vazante	Pamplona	CMM-500	I	32	-2.4	-2.3		55.72	44.28	128	70	3184	0.709350	0.000009	1.8	0.014
KV-500-3	Vazante	Pamplona	CMM-500	I	76	-6.9	-0.7	11.9	55.44	44.56	60	41	1308	0.707247	0.000007	1.5	0.025
KV-500-4	Vazante	Pamplona	CMM-500	I	138	-7.0	-0.8		53.63	46.37	38	38	1522			1.0	
KV-500-5	Vazante	Pamplona	CMM-500	I	173	-4.8	0.7		54.94	45.06	148	49	2294	0.710601	0.000008	3.0	0.021
KV-500-7	Vazante	Pamplona	CMM-500	I	286	-4.3	1.9		56.35	43.65	202	43	1438	0.708113	0.000008		0.023
KV-244-3	Vazante	Pamplona	CMM-244	I	40	-4.4	2.0		55.21	44.79	391	46	5009	0.712227	0.000009	8.5	0.022
KV-244-3	Vazante	Pamplona	CMM-244	III	40	-6.4	2.1		55.05	44.95	686	57	7564			5.4	
KV-244-6	Vazante	Pamplona	CMM-244	I	70	-5.4	1.7		54.24	45.82	182	34	3998				
KV-244-6	Vazante	Pamplona	CMM-244	IV	70	-8.9	1.5		56.11	43.89	487	34	9330				
KV-244-9	Vazante	Pamplona	CMM-244	I	96	-5.9	2.3		56.23	43.77	338	46	4414	0.709666	0.000008	7.4	0.022
KV-244-9	Vazante	Pamplona	CMM-244	III	96	-5.6	1.6		55.86	44.14	879	57	5224				
KV-244-9	Vazante	Pamplona	CMM-244	IV	96	-10.3	2.0		56.67	43.33	973	32	13034	0.708526	0.000008		0.031
KV-244-11	Vazante	Pamplona	CMM-244	I	118	-6.1	2.0	8.5	54.63	45.37	329	42	3987	0.708294	0.000008	7.8	0.024
KV-244-21	Vazante	Pamplona	CMM-244	I	209	-4.8	1.8		57.59	42.41	225	62	3685	0.711934	0.000008	3.6	0.016
KV-244-21	Vazante	Pamplona	CMM-244	II B	209	-5.9	2.3		56.08	43.92	96	40	1680				
KV-244-24	Vazante	Pamplona	CMM-244	I	241	-4.9	2.4	9.9	55.68	44.32	218	56	13684	0.721312	0.000008	3.9	0.018
KV-244-24	Vazante	Pamplona	CMM-244	III	241	-5.2	1.6		56.79	43.21	642	74	7426				
KV-244-26	Vazante	Pamplona	CMM-244	I	255	-5.8	2.0		55.33	44.67	315	60	14492	0.709710	0.000008	5.3	0.017
KV-244-26	Vazante	Pamplona	CMM-244	II A	255	-5.0	2.6		57.39	42.61	310	49	2787				
KV-244-26	Vazante	Pamplona	CMM-244	II B	255	-5.2	2.0		55.39	44.61	459	58	3484				
KV-244-26	Vazante	Pamplona	CMM-244	IV	255	-8.6	0.2		57.78	42.22	2094	31	17297	0.710910	0.000008		0.032
KV-244-27	Vazante	Pamplona	CMM-244	I	263	-5.0	2.6		55.05	44.95	20	48	5392	0.714138	0.000008	0.4	0.021
KV-244-27	Vazante	Pamplona	CMM-244	II B	263	-5.5	1.4		56.15	43.85	529	49	6176				
KV-244-29	Vazante	Pamplona	CMM-244	I	306	-4.2	2.0		55.14	44.86	222	34	4312	0.713735	0.000008	6.5	0.029
KV-244-29	Vazante	Pamplona	CMM-244	II B	306	-6.3	1.7		56.70	43.30	449	36	7912				
KV-244-29	Vazante	Pamplona	CMM-244	IV	306	-11.2	1.5		57.22	42.78	1082	24	22009	0.711131	0.000009		0.042
KV-244-30	Vazante	Pamplona	CMM-244	I	335	-4.8	1.1		55.36	44.64	166	65	3522	0.714660	0.000008	2.5	0.015
KV-244-30	Vazante	Pamplona	CMM-244	III	335	-5.2	1.6		56.35	43.65	737	83	3326	0.715374	0.000008		0.012
KV-244-31	Vazante	Pamplona	CMM-244	I	350	-5.6	1.4		55.76	44.24	110	81	3666	0.731601	0.000009	1.4	0.012
KV-244-35	Vazante	rr do Pin	CMM-244	I	420	-4.0	1.0		55.69	44.31	262	81	3945	0.719673	0.000009	3.2	0.012
KV-244-35	Vazante	rr do Pin	CMM-244	IV	420	-9.7	1.2		57.68	42.32	1033	50	11400				
KV-244-38	Vazante	rr do Pin	CMM-244	I	467	-5.0	0.8	10.8	56.01	43.99	201	106	4941	0.731567	0.000009	1.9	0.009
KV-244-40	Vazante	rr do Pin	CMM-244	I	481	-3.3	2.0		56.02	44.98	69	65	4715			1.1	

Field No.	Formatio	Member	Core	Dolomite	Depth (m)	$\delta^{18}O$	$\delta^{13}C$	$\delta^{34}S$	CaCO <sub>3</sub> %	MgCO <sub>3</sub> %	Mn(ppm)	Sr(ppm)	Fe(ppm)	<sup>87</sup> Sr/ <sup>86</sup> Sr	$\pm 2\sigma$	Mn/Sr	I/Sr
KV-244-42	Vazante	rr do Pin	CMM-244	I	499	-2.6	1.6		56.46	43.54	28	42	2056	0.709958	0.000008	0.6	0.024
KV-244-44	Vazante	rr do Pin	CMM-244	I	514	-2.9	1.3		56.00	44.00	21	75	1440	0.710715	0.000008		0.013
KV-244-44	Vazante	rr do Pin	CMM-244	II A	514	-2.2	2.3		55.49	44.51	82	36	644	0.710575	0.000007	2.3	0.028
KV-244-44	Vazante	rr do Pin	CMM-244	II A	514	-3.6	2.0		55.45	44.55	109	36	1081				
KV-244-45	Vazante	rr do Pin	CMM-244	I	530	-3.3	1.5		57.92	42.08	304	51	6915			5.9	
KV-244-46	Vazante	rr do Pin	CMM-244	I	543	-2.9	1.7		56.91	43.09	87	45	1251	0.711024	0.000008	1.9	0.022
KV-244-47	Vazante	rr do Pin	CMM-244	I	553	-5.3	1.7		54.90	45.10	23	50	3120			0.5	
KV-244-47	Vazante	rr do Pin	CMM-244	II A	553	-1.8	1.7		56.23	43.77	114	44	953				
KV-244-47	Vazante	rr do Pin	CMM-244	II B	553	-4.2	1.6		57.34	42.66	212	46	1790				
KV-244-47	Vazante	rr do Pin	CMM-244	IV	553	-8.8	1.6		57.66	42.34	217	21	18014	0.716559	0.000009		0.048
KV-244-48	Vazante	rr do Pin	CMM-244	I	566	-5.2	1.8		54.63	45.37	101	37	2808	0.711393	0.000008	2.7	0.027
KV-244-48	Vazante	rr do Pin	CMM-244	IV	566	-10.2	1.5		54.61	45.39	263	29	6787				
KV-244-48	Vazante	rr do Pin	CMM-244	IV	566	-9.2	1.7		55.05	44.95	206	18	7995	0.715139	0.000008		0.056
KV-244-51	Vazante	rr do Pin	CMM-244	I	609	-3.7	1.0		56.39	43.61	96	51	1346	0.713517	0.000008	1.9	0.020
KV-244-54	Vazante	rr do Pin	CMM-244	I	647	-3.9	1.3		55.38	44.62	103	62	1631			1.7	
KV-244-54	Vazante	rr do Pin	CMM-244	IV	647	-10.1	1.4		56.39	43.61	798	34	7911	0.709630	0.000008		0.029
KV-244-54	Vazante	rr do Pin	CMM-244	IV	647	-9.1	1.4		56.81	43.19	868	34	9727				
KV-244-57	Vazante	rr do Pin	CMM-244	I	688	-3.9	1.6		56.32	43.68	96	42	2817	0.708188	0.000012	2.3	0.024
KV-244-59	Vazante	rr do Pin	CMM-244	I	723	-5.2	1.8	16.5	57.92	42.08	139	41	1443	0.707949	0.000008	3.4	0.024
KV-244-61	Vazante	rr do Pin	CMM-244	I	756	-3.3	2.1		57.06	42.94	392	48	3784	0.710980	0.000008	8.2	0.021
KV-244-61	Vazante	rr do Pin	CMM-244	IV	756	-7.8	1.8		56.31	43.69	417	66	2135				
KV-244-61	Vazante	rr do Pin	CMM-244	IV	756	-12.0	1.2		55.95	44.05	614	110	6921	0.725232	0.000009		0.009
KV-244-63	Vazante	rr do Pin	CMM-244	I	783	-7.3	1.5		55.34	44.66	234	30	2555			7.9	
KV-244-64	Vazante	rr do Pin	CMM-244	I	803	-6.8	0.9		55.08	44.92	183	22	1997	0.707344	0.000008	8.3	0.045
KV-244-67	Vazante	rr do Pin	CMM-244	I	847	-2.5	1.8	12.3	56.23	43.77	117	28	1426	0.708138	0.000008	4.2	0.036
KV-244-69	Vazante	rr do Pin	CMM-244	I	877	-4.1	2.1		56.44	43.56	114	34	1173	0.710947	0.000008	3.4	0.030
KV-244-71	Vazante	rr do Pin	CMM-244	I	919	-5.5	2.3		56.19	43.81	19	28	1576	0.712911	0.000008	0.7	0.036
KV-244-75	Vazante	rr do Pin	CMM-244	I	1023	-5.8	1.9		55.18	44.82	255	34	3159	0.714346	0.000008	7.5	0.030
KV-244-78	Vazante	rr do Pin	CMM-244	I	1100	-0.1	3.9		54.59	45.41	81	54	1729	0.713312	0.000008	1.5	0.018
KV-244-78	Vazante	rr do Pin	CMM-244	IV	1100	-8.2	1.7		56.35	43.65	823	70	9535				
KV-244-80	rra do Garrote	rr do Pin	CMM-244	I	1122	-4.4	1.4		55.61	44.39	163	68	1642	0.716098	0.000008	2.4	0.015
KV-244-80	rra do Garrote	rr do Pin	CMM-244	IV	1122	-9.7	0.5		57.15	42.85	897	37	11694				
LS2	(limes) rra do Garrote	Field sampl		I	?	-6.8	3.2	16.9	98.61	1.39	35	1466		0.706986	0.000008	0.0	0.001
LS1	(limes) rra do Garrote	Field sampl		I	?	-7.6	3.3	14.2	98.50	1.50	75	1469		0.706901	0.000007	0.1	0.001

I = mainly microbial mud matrix, II = fibrous cement (generation A and B), III = equant cement, IV = latest and fracture-filling saddle dolomite. The  $\delta^{34}S$  values represent whole-rock, mainly algae and algal matrix, analysis and highlighted values are total sulfur isotope analysis

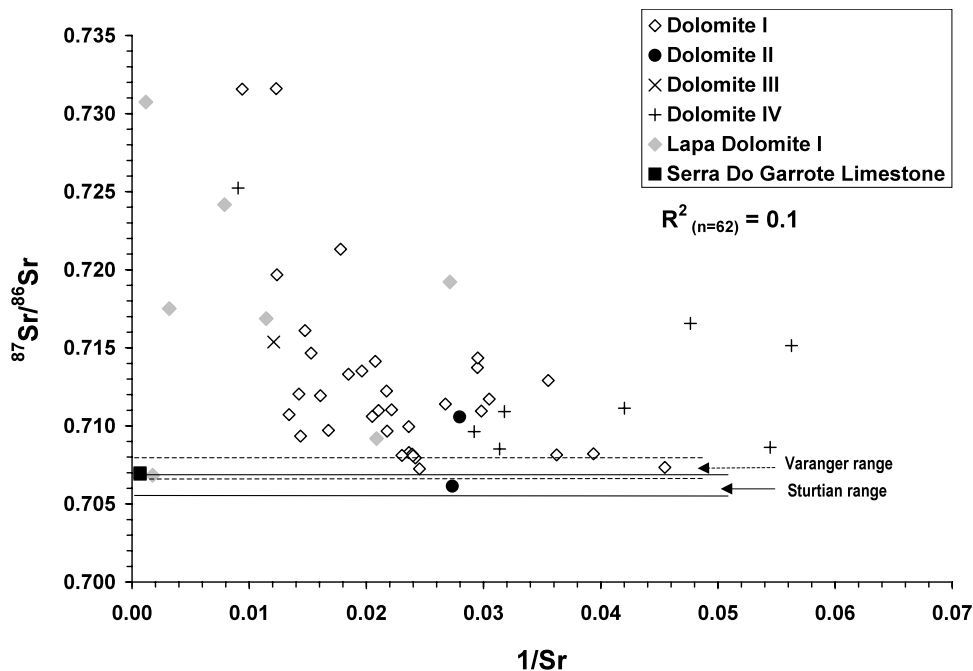


Fig. 13. Crossplot of  $1/Sr$  vs.  $^{87}Sr/^{86}Sr$  for all studied carbonates from the Vazante area. The ranges of values for the Varanger and Sturtian time intervals are from Jacobsen and Kaufman (1999).

## References

- Al-Aasm, I.S., Azmy, K., 1996. Diagenesis and evolution of microporosity of Middle-Upper Devonian Kee Scarp Reefs, Norman Wells, Northwest Territories, Canada: petrographic and geochemical aspects. *AAPG Bull.* 80, 82–100.
- Al-Aasm, I.S., Lu, F., 1994. Multistage dolomitization of the Mississippian Turner Valley Formation, Quirk Creek Field, Alberta: chemical and petrologic evidence. *Pangea: Global Environments and Resources*, Canadian Society of Petroleum Geologists. *Memoir* 17, 657–675.
- Alkmim, F.F., Brito Neves, B.B., Alves, J.A.C., 1993. Arcabouço tectônico do Craton do São Francisco, Uma revisão. In: Dominguez, J.M.L., Misi, A. (Eds.), *O Craton do São Francisco, SBG BA-SE/SGM/CNPq*. Salvador, BA, Brazil, pp. 45–62.
- Almeida de, F.F.M., Hasui, Y., 1984. In: Blucher, E. (Ed.), *O Precambriano do Brasil*, São Paulo, p. 377.
- Almeida, F.F.M., Hasui, Y., Breto Neves, B.B., 1976. The upper Precambrian of South America. *Bol. Inst. Geocienc. Univ. São Paulo* 7, 45–80.
- Amaral, G., Kawashita, K., 1967. Determinação do idade do Grupo Bambuí, *Inst. Geociencias Univ. Parana. Pub. No.* 26, 39–40.
- Arvidson, R., Mackenzie, F.T., 1997. Tentative kinetic model for dolomite precipitation rate and its application to dolomite distribution. *Aquat. Geochem.* 2, 273–298.
- Arvidson, R., Mackenzie, F.T., 1999. The dolomite problem: control of precipitation kinetics by temperature and saturation state. *Am. J. Sci.* 299, 257–288.
- Asmerom, Y., Jacobsen, S.B., Knoll, A.H., Butterfield, N.J., Swett, K., 1991. Strontium isotopic variations of Neoproterozoic seawater: implications for crustal evolution. *Geochim. Cosmochim. Acta* 55, 2883–2894.
- Azmy, K., Veizer, J., Bassett, M., Copper, P., 1998. Oxygen and carbon isotopic composition of Silurian brachiopods: implications for coeval seawater and glaciations. *GSA Bull.* 110, 1499–1512.
- Azmy, K., Veizer, J., Wenzel, B., Bassett, M.G., Copper, P., 1999. Silurian strontium isotope stratigraphy. *GSA Bull.* 111, 475–483.
- Babinski, M., Van Schum, W.R., Chemale, F. Jr, 1999. Pb-Pb dating and Pb isotope geochemistry of Neoproterozoic carbonate rocks from São Francisco basin, Brazil: implications for the mobility of Pb isotopes during tectonism and metamorphism. *Chem. Geol.* 160, 175–199.
- Banner, J.L., 1995. Application of the trace element and isotope geochemistry of strontium to studies of carbonate diagenesis. *Sedimentology* 42, 805–824.
- Banner, J.L., Hanson, G.N., 1990. Calculations of simultaneous isotopic and trace element variations during water-rock interaction with applications to carbonate diagenesis. *Geochim. Cosmochim. Acta* 54, 3123–3137.
- Bose, P.K., Sarkar, S., Bhattacharyya, S.K., 1996. Dissolution seams: some observations from the Proterozoic Chanda

- Limestone, Adilabad, India. Carbonates Evaporites 11, 70–76.
- Brand, U., Veizer, J., 1980. Chemical diagenesis of a multi-component carbonate system-1: trace elements. *J. Sed. Petrol.* 50, 1219–1236.
- Budd, D.A., 1997. Cenozoic dolomites of carbonate islands: their attributes and origin. *Earth-Sci. Rev.* 42, 1–47.
- Burdett, J.W., Grotzinger, J.P., Arthur, M.A., 1990. Did major changes in the stable isotope composition of Proterozoic seawater occur? *Geology* 18, 227–230.
- Chemale, F. Jr, Alkmim, F.F., Endo, I., 1993. Late Proterozoic tectonism in the interior of the São Francisco craton. In: Findlay, R.H., Unrug, R., Banks, M.R., Veever, J.J. (Eds.), *Gondwana Assembly—Assembly, Evolution and Dispersal*. Balkema, Rotterdam, pp. 29–42.
- Choquette, P.W., James, N.P., 1987. Diagenesis # 12 in Limestones-3. The deep burial environment. *Geosci. Can.* 14, 3–36.
- Clark, I.D., Fritz, P., 1997. *Environmental Isotopes in Hydrogeology*. Lewis publisher, Boca Raton, p. 328.
- Claypool, G.E., Holser, W.T., Kaplan, I.R., Sakai, H., Zak, I., 1980. The age curves of sulfur and oxygen isotopes in marine sulfate and their mutual interpretation. *Chem. Geol.* 28, 190–260.
- Cloud, P.E., Dardenne, M.A., 1973. Proterozoic age of the Bambuí Group in Brazil. *GSA Bull.* 84 (5), 1673–1676.
- Coleman, M.L., Walsh, J.N., Benmore, R.A., 1989. Determination of both chemical and stable isotope composition in milligram-size carbonate samples. *Sed. Geol.* 65, 233–238.
- Corsetti, F.A., Kaufman, A.J., 1994. Chemostratigraphy of Neoproterozoic-Cambrian Units, White-Inyo Region, eastern California: Implications for Global Correlation and Faunal Distribution. *Palios* 9, 211–219.
- Dardenne, M.A., 1978. Sentese sobre a estratigráfico Grupo Bambuí no Brasil Central. *Anais do XXX Cong. Bras. Geol.* 2, 597–610.
- Dardenne, M.A., 1979. Les Mineralisations de Plomb, Zinc, Fluor du Proterozoïque Supérieur dans le Brésil Central, 'Docteur es Sciences' Thesis, University Pierre & Marie Curie (Univ. of Paris VI), p. 251.
- Dardenne, M.A., Walde, D.H.G., 1979. A estratigrafia dos Grupos Bambuí e Macaúbas no Brasil Central. *Bol. Soc. Bras. Geol. Núcleo Minas Gerais* 1, 43–53.
- Dardenne, M.A., Freitas-Silva, F.H., Souza, J.C.F., Campos, J.E.G., 1998. Avaliação tectono-sedimentar do Grupo Vazante no contexto da faixa de dobramentos Brasília. *Anais do XL Congresso Brasileiro de Geologia, Belo Horizonte, MG (Brasil), Anais (Proceedings)*, p. 26.
- D'Agrella-Fihlo, M.S., Babinski, M., Trindade, R.I.F., Van Schmus, W.R., Ernesto, M., 2000. Simultaneous remagnetization and U–Pb isotope resin Neoproterozoic carbonates of the São Francisco craton. *Brazil. Precambrian Res.* 99, 179–196.
- Dawans, J.M., Swart, P.K., 1988. Textural and geochemical alternations in late Cenozoic: Bahamian dolomites. *Sedimentology* 35, 385–404.
- De Oliveira, T.F., 1998. Cia Mineira de Metais, P.O. Box # 1, 38780-Vazante-MG-Brazil.
- Derry, L.A., Keto, L.S., Jacobsen, S.B., Knoll, A.H., Swett, K., 1989. Sr isotopic variations of upper Proterozoic carbonates from East Greenland and Svalbard. *Geochim. Cosmochim. Acta* 53, 2331–2339.
- Derry, L.A., Kaufman, A.J., Jacobsen, S.B., 1992. Sedimentary cycles and environmental change in the Late Proterozoic: evidence from stable and radiogenic isotopes. *Geochim. Cosmochim. Acta* 56, 1317–1329.
- Derry, L.A., Brasier, M.D., Corfield, R.M., Rozanov, A.Y.u., Zhuravlev, A.Y.u., 1994. Sr and C isotopes in Lower Cambrian carbonates from Siberian craton: a paleoenvironmental record during the Cambrian explosion. *Earth Planet. Sci. Lett.* 128, 671–681.
- Dickson, J.A.D., 1966. Carbonate identification and genesis as revealed by staining. *J. Sed. Petrol.* 36, 491–505.
- Diener, A., Ebner, S., Veizer, J., Buhl, D., 1996. Strontium isotope stratigraphy of the Middle Devonian: brachiopods and conodonts. *Geochim. Cosmochim. Acta* 60, 639–652.
- Drever, J.I., 1988. *The Geochemistry of Natural Waters*. Prentice Hall, Englewood Cliffs, NJ, p. 437.
- Fairchild, I.J., 1991. Origins of carbonates in Neoproterozoic stromatolites and identification of modern analogues. *Precambrian Res.* 53, 281–299.
- Fairchild, I.J., Spiro, B., 1987. Petrological and isotopic implications of some contrasting Late Precambrian carbonates, NE Spitsbergen. *Sedimentology* 34, 973–989.
- Fairchild, I.J., Spiro, B., 1990. Carbonate in Glacial sediments: geochemical clues to paleoenvironment. In: Dowdeswell, A.J., Scourse, J.D. (Eds.), *Glacimarine Environment: Process and Sediments*. Geol. Soc. Spec. Publication 53, 201–216.
- Fairchild, I.J., Marshall, J.D., Bertrand-Safati, J., 1990. Stratigraphic shifts in carbon isotopes from Proterozoic stromatolitic carbonates (Mauritania): influence of primary mineralogy and diagenesis. *Am. J. Sci.* 290-A, 46–79.
- Fairchild, I.J., Knoll, A.H., Keene, S., 1991. Coastal lithofacies and biofacies associated with syndepositional dolomitization and silicification (Draken Formation, Upper Riphean, Svalbard). *Precambrian Res.* 53, 165–197.
- Fairchild, T.R., Schopf, J.W., Shen-Miller, J., Guimaraes, E.M., Edwards, M.D., Lagstein, A., Li, X., Pabst, M., De Melo-Filho, L.S., 1996. Recent discoveries of Proterozoic microfossils in south-central Brazil. *Precambrian Res.* 80, 125–152.
- Fairchild, I.J., Spiro, B., Herrington, P., Song, T., 2001. Geological controls on Sr and C isotope compositions on Neoproterozoic Sr-rich limestones of E. Greenland and N. China. In: Grotzinger, J.P., James, N.P. (Eds.), *Carbonate sedimentation and diagenesis in the evolving Precambrian World*. SEPM Special Publication 67, 297–313.
- Freitas-Silva, F.H., Dardenne, M.A., 1992. Quadro estratigráfico das Formações Paracatu e Vazante na Rigião de paracatu-MG-Rvista da Escola de Minas. *Ouro Preto* 45 (1/2), 57–59.
- Goldstein, R.H., Reynolds, T.J., 1994. Systematics of fluid inclusions in diagenetic minerals, Short course 31, SEPM (Society for Sedimentary Geology), p. 199.



- Gorkhov, I.M., Semikhatov, M.A., Baskakov, A.V., Kutvavin, E.P., Mel'nikov, N.N., Sochava, A.V., Turchenko, T.L., 1995. Sr isotope composition in Riphean, Vendian, and lower Cambrian carbonates from Siberia. *Stratigr. Geol. Correl.* 3, 1–28.
- Hall, G.E.M., Pelchat, J.-C., Loop, J., 1988. Separation and recovery of various sulphur species in sedimentary rocks for stable sulphur isotopic determination. *Chem. Geol.* 67, 35–45.
- Hitzman, M.W., Fogarty, C.F., 1997. Observations from the Vaznte Zinc Mine, Minas Gerais, Brazil. Colorado school of mines, unpublished report.
- Hoffman, P.F., 1991. Did the breakout of Laurentia turn Gondwanaland inside-out. *Science* 252, 1409–1412.
- Hoffman, P.F., Kaufman, A.J., Halverson, G.P., 1998. Comings and goings of global glaciation on a Neoproterozoic tropical platform in Namibia. *GSA Today* 8, 1–9.
- Holser, W.T., Schidlowski, M., MacKenzie, F.T., Maynard, J.B., 1988. Geochemical cycles of carbon and sulfur. In: Gregor, C.B., Garrels, R.M., MacKenzie, F.T., Maynard, J.B. (Eds.), *Chemical Cycles in the Evolution of the Earth*. Wiley, New York, p. 276.
- Iyer, S.S., Hoefs, J., Krouse, H.R., 1992. Sulfur and lead isotope geochemistry of galena from the Bambuí Group, Minas Gerais, Brazil-implications for ore genesis. *Econ. Geol.* 87, 437–443.
- Iyer, S.S., Babinski, M., Krouse, H.R., Chemale, F. Jr, 1995. Highly  $^{13}\text{C}$ -enriched carbonate and organic matter in the Neoproterozoic sediments of the Bambuí Group. *Brazil. Precambrian Res.* 73, 271–282.
- Jacobsen, S.B., Kaufman, A.J., 1999. The Sr, C and O isotope evolution of Neoproterozoic seawater. *Chem. Geol.* 161, 37–57.
- Karfunkel, J., Hoppe, A., 1988. Late Proterozoic glaciation in central-eastern Brazil: synthesis and model. *Paleogeogr. Paleoclimat. Plaeoecol.* 65, 1–21.
- Kaufman, A.J., Hayes, J.M., Knoll, A.H., Germs, G.J.B., 1991. Isotopic compositions of carbonates and organic carbon from upper Proterozoic successions in Namibia: stratigraphic variation and the effect of diagenesis and metamorphism. *Precambrian Res.* 49, 301–327.
- Kaufman, A.J., Jacobsen, S.B., Knoll, A.H., 1993. The Vendian record of Sr- and C-isotopic variations in seawater: implications for tectonics and paleoclimate. *Earth Planet. Sci. Lett.* 120, 409–430.
- Kaufman, A.J., Knoll, A.H., 1995. Neoproterozoic variations in the C-isotopic composition of seawater: stratigraphic and biogeochemical implications. *Precambrian Res.* 73, 27–49.
- Kaufman, A.J., Knoll, A.H., Awramik, S.M., 1992. Biostratigraphic and chemostratigraphic correlation of Neoproterozoic sedimentary successions: Upper Tindir Group, northwestern Canada, as a test case. *Geology* 20, 181–185.
- Kaufman, A.J., Knoll, A.H., Semikhatov, M.A., Grotzinger, J.P., Jacobsen, S.B., Adams, W., 1996. Integrated chronostratigraphy of Proterozoic-Cambrian boundary beds in the western Anabar region, northern Siberia. *Geol. Mag.* 133, 509–533.
- Kaufman, A.J., Knoll, A.H., Narbonne, G.M., 1997. Isotopes, ice ages and terminal Proterozoic Earth history. *Proc. Natl. Acad. Sci.* 94, 6600–6605.
- Kawashita, K., 1998. Rochas carbonáticas neoproterozóicas da América do Sul: idadese inferências quimioestratigráficas. Unpublished Pos Doctoral Thesis (LD), University of São Paulo, SP, Brazil, p. 126.
- Knoll, A.H., Walter, M.R., 1992. Latest Proterozoic stratigraphy and Earth history. *Nature* 356, 673–678.
- Knoll, A.H., Hayes, J.M., Kaufman, A.J., Swett, K., Lambert, I.B., 1986. Secular variations in carbon isotope ratios from Upper Proterozoic successions of Svalbard and East Greenland. *Nature* 321, 832–838.
- Lagoeiro, L.E., 1990. Estudo da deformação nas sequências carbonáticas do Grupo Una na região de Irecê. BA Msc Dissertation, Universidade Federal de Ouro Preto, Brazil.
- Land, L.S., 1983. The application of stable isotopes to studies of the origin of dolomite and to problems of diagenesis of clastic sediments. In: Arthur, M.A., Anderson, T.F., Kaplan, I.R., Veizer, J., Land, L.S. (Eds.), *Stable Isotopes in Sedimentary Geology*. SEPM Short Course Notes 10, 4-1–4-22.
- Land, L.S., 1992. The dolomite problem: stable and radiogenic isotope clues. In: Clauer, N., Chaudhuri, S. (Eds.), *Isotopic Signature of Sedimentary Records*. Lecture Notes in Earth Science 43, 49–68.
- Li, Z.X., Zhang, L., McPowell, C.M., 1995. South China in Rodinia: part of the missing link between Australia-East Antarctica and Laurentia. *Geology* 23, 407–410.
- Lohmann, K.C., 1988. Geochemical patterns of meteoric diagenetic systems and their applications to studies of paleokarst. In: Choquette, P.W., James, N.P. (Eds.), *Paleokarst*. Springer, Berlin, pp. 55–80.
- Lohman, K.C., Walker, J.C.G., 1989. The  $\delta^{18}\text{O}$  record of Phanerozoic abiotic marine calcite cements. *Geophys. Res. Lett.* 16, 319–322.
- Macedo, M.H.F., Bonhomme, M.G., 1984. Contribuição à cronoestratigrafia das formações Caboclo, Babedouro e Salitre na Chapada Diamantina (BA) pelos métodos Rb-Sr e K-Ar. *Rev. Brasil. Geociên.* 14, 153–163.
- Machel, H.G., Mountjoy, E.W., 1986. Chemistry and environments of dolomitization- a reappraisal. *Earth-Sci. Rev.* 23, 175–202.
- Madalosso, A., 1979. Stratigraphy and sedimentation of the Bambuí Group in Paracatu region, Minas Gerais. Brazil. MSc. Thesis, University of Missouri, p. 127.
- Maliva, R.G., 1998. Skeletal aragonite neomorphism-quantitative modelling of two-water diagenetic system. *Sed. Geol.* 121, 179–190.
- McArthur, J.M., 1994. Recent trends in strontium isotope stratigraphy. *Terra Nova* 6, 331–358.
- McKirdy, D.M., Burgess, J.M., Lemon, N.M., Yu, X., Cooper, A.M., Gostin, V.A., Jenkins, R.J.F., Both, R.A., 2001. A chemostratigraphic overview of the late Cryogenian interglacial sequence in the Adelaide Fold-Thrust Belt, South Australia. *Precambrian Res.* 106, 149–186.

- Meert, J.G., Van der Voo, R., 1994. The Neoproterozoic (1000–540 Ma) glacial intervals: no more snowball Earth? *Earth and Planet. Science. Lett.* 123, 1–13.
- Misi, A., Kyle, J.R., 1994. Upper Proterozoic carbonate stratigraphy, diagenesis, and stromatolitic phosphorite formation, Irecê Basin, Bahia, Brazil. *J. Sed. Res.* 64 (3), 299–310.
- Misi, A., Veizer, J., 1998. Neoproterozoic carbonate sequences of the Una Group, Irecê Basin, Brazil: chemostratigraphy, age and correlations. *Precambrian Res.* 89, 87–100.
- Misi, A., Veizer, J., Kawashita, K., Dardenne, M.A., 1997. The age of the Neoproterozoic carbonate platform sedimentation based on  $^{87}\text{Sr}/^{86}\text{Sr}$  determinations, Bambuí and Una groups, Brazil. *South-American Symposium on Isotope Geology, Brazil*, pp. 199–200.
- Narbonne, G.M., Aitken, J.D., 1995. Neoproterozoic of the Mackenzie Mountains northwestern Canada. *Precambrian Res.* 73, 101–121.
- Narbonne, G.M., Kaufman, A.J., Knoll, A.H., 1994. Integrated chemostratigraphy and biostratigraphy of the Windermere Supergroup, northern Canada: implications for Neoproterozoic correlations and early evolution of animals. *GSA Bull.* 106, 1281–1292.
- Parenti Couto, M.R., Cordani, U.G., Kawashita, A.K., Iyer, S.S., Moraes, N.M.P., 1981. Considerações sobre a idade do Grupo Bambuí com base em análises isotópicas de Sr e Pb. *Rev. Bras. Geociên.* 11, 5–16.
- Park, J.K., Buchan, K.L., Harlan, S., 1995. A proposed giant radiating dyke swarm fragmented by the separation of Laurentia and Australia based paleomagnetism of ca. 780 Ma mafic intrusions in western North America. *Earth Planet Sci. Lett.* 132, 129–139.
- Pedrosa Soares, A.C., Dardenne, M.A., Hasui, Y., Castro, F.D.C., Carvalho, M.V.A., Reis, A.C., 1994. Mapa Geológico do Estado de Minas Gerais e Nota Explicativa, Secretaria de Recursos Minerais, Hídricos e Energéticos, Companhia Mineradora de Minas Gerais (COMIG), maps, p. 97.
- Pelechaty, S.M., Kaufman, A.J., Grotzinger, J.P., 1996. Evaluation of  $\delta^{13}\text{C}$  chemostratigraphy for basinal correlation: Vendian strata of northeast Siberia. *GSA Bull.* 108, 992–1003.
- Pratt, B.R., James, N.P., Clinton, A.C., 1992. Peritidal carbonates. In: Walker, R.G., James, N.P. (Eds.), *Facies Models: Response to Sea Level Change*. Geological Association of Canada, Canada, p. 409.
- Rigobello, A.E., Branquinho, J.A., Dantas, M.G., De Oliveira, T.F., Filho, W.N., 1988. Mina de Zinco de Vazante. In: Schobbenhaus, C., Coelho, C.E (Eds.), *Principais Depósitos Minerais do Brasil*. DNPM/CVRD 3, 111–121.
- Ross, G.M., 1999. Paleogeography: an earth systems perspective. *Chem. Geol.* 161 (1–3), 5–16.
- Sarkar, S., Chakraborty, P.P., Bhattacharya, S.K., Banerjee, S., 1998. C12-enrichment along intraformational unconformities within Proterozoic Bhandar limestone, Son Valley, India and its implications. *Carbonates Evaporites* 13, 108–114.
- Saylor, B.Z., Kaufman, A.J., Grotzinger, J.P., Urban, F., 1998. A composite reference section for terminal Proterozoic strata of southern Namibia. *J. Sed. Res.* 68, 1223–1235.
- Schidlowski, M., 1989. Evolution of the sulphur cycle in the Precambrian. In: Brimblecombe, P., Yu. Lein, A. (Eds.), *Evolution of the Global Biogeochemical Sulphur Cycle*. Wiley, New York, pp. 3–19.
- Schidlowski, M., Hayes, J.M., Kaplan, I.R., 1983. Isotopic interference of ancient biomicrites: carbon, sulfur, hydrogen, and nitrogen. In: Schopf, J.W. (Ed.), *Earth's Earliest Biosphere: Its Origin and Evolution*. Princeton Univ. Press, Princeton, NJ, pp. 149–186.
- Schmidt, P.W., Williams, G.E., 1995. The Neoproterozoic climatic paradox: equatorial paleolatitude for Marinoan glaciation near sea level in Australia. *Earth Planet. Sci. Lett.* 134, 107–124.
- Sheppard, S.M.F., Schwarcz, H.P., 1970. Fractionation of carbon and oxygen isotopes and magnesium between coexisting metamorphic calcite and dolomite. *Contrib. Mineral. Petrol.* 26, 161–198.
- Shieh, Y.N., Taylor, H.P., 1969. Oxygen and carbon isotope studies of contact metamorphism of carbonate rocks. *J. Petrol.* 10, 307–331.
- Sibley, D.F., 1982. Origin of common dolomite fabrics: clues from the Pliocene. *J. Sed. Petrol.* 52, 1087–1100.
- Sibley, D.F., Gregg, J.M., 1987. Classification of dolomite rock textures. *SEPM* 57, 967–975.
- Strauss, H., 1993. The sulfur isotopic record of Precambrian sulfates: new data and a critical evaluation of the existing record. *Precambrian Res.* 63, 225–246.
- Strauss, H., 1997. The isotopic composition of sedimentary sulfur through time. *Paleogeogr. Paleoclim. Paleoecol.* 132, 97–118.
- Thomaz Filho, A., Lima, V.Q., 1981. Datação radiométrica de rochas pelicas pelo método Rb–Sr. *Boletim Petrobrás* 24, 109–119.
- Thomaz Filho, A., Kawashita, K., Cordani, U.G., 1998. A origem do Grupo Bambuí no contexto da evolução geotectônica e de idades radiométricas. *Ann. Acad. Bras. Ciên.* 70 (3), 527–548.
- Torsvik, T.H., Smethurst, M.A., Meert, J.G., Van der Voo, R., McKerrow, W.S., Brasier, M.D., Sturt, B.A., Walderhaug, H.J., 1996. Continental break-up and collision in Neoproterozoic and Paleozoic—a tale of Baltica and Laurentia. *Earth Sci. Rev.* 40, 229–258.
- Tucker, M.E., Wright, V.P., 1990. *Carbonate Sedimentology*. Blackwell Scientific, Oxford, p. 482.
- Ussami, N., 1993. Estudos Geofísicos no Craton do São Francisco: Estágio Atual e Perspectivas. In: *O Craton do São Francisco-Trabalhos Apresentados na Reunião Preparatória do II Simpósio sobre o Craton do São Francisco*. Salvador, Ba, pp. 35–43.
- Vahrenkamp, V.C., Stewart, P.K., 1990. A new distribution coefficient for the incorporation of strontium into dolomite and its implications for the formation of ancient dolomites. *Geology* 18, 387–391.
- Veizer, J., 1983. Chemical diagenesis of carbonates: Theory and application of trace element technique. In: Arthur,

- M.A., Anderson, T.F., Kaplan, I.R., Veizer, J., Land, L.S. (Eds.), *Stable Isotopes in Sedimentary Geology*. Society of Economic Paleontologists and Mineralogists (SEPM) Short Course Notes 10, III-1–III-100.
- Veizer, J., Compston, W., 1976.  $^{87}\text{Sr}/^{86}\text{Sr}$  in Precambrian carbonates as an index of crustal evolution. *Geochim. Cosmochim. Acta* 40, 905–914.
- Veizer, J., Bruckschen, P., Pawellek, F., Podlaha, O., Jasper, T., Korte, C., Strauss, H., Azmy, K., Ala, D., 1997. Oxygen isotope evolution of Phanerozoic seawater. *Palaeogeogr. Palaeoclimat. Palaeoecol.* 132, 159–172.
- Veizer, J., Ala, D., Azmy, K., Bruckschen, P., Bruhn, F., Buhl, D., Carden, G., Diener, A., Ebner, S., Goddard, Y., Jasper, T., Korte, C., Pawellek, F., Podlaha, O., Strauss, H., 1999.  $^{87}\text{Sr}/^{86}\text{Sr}$ ,  $\delta^{18}\text{O}$  and  $\delta^{13}\text{C}$  evolution of Phanerozoic seawater. *Chem. Geol.* 161, 59–88.
- Walter, M.R., Veevers, J.J., Calver, C.R., Gorjan, P., Hill, A.C., 2000. Dating the 840–544 Ma Neoproterozoic interval by isotopes of strontium, carbon, and sulfur in seawater, and some interpretative models. *Precambrian Res.* 100, 371–433.
- Wenzel, B., 2000. Differential preservation of primary isotopic signature in Silurian brachiopods from northern Europe. *J. Sed. Res.* 70, 194–209.
- Wickham, S.M., Peter, M.T., 1993. High  $\delta^{13}\text{C}$  Neoproterozoic carbonate rocks in western North America. *Geology* 21, 165–168.